Generation of ORIGEN Reactor Libraries for Liquid-Fueled Molten Salt Reactors

A Thesis Presented for the

Master of Science

Degree

The University of Tennessee, Knoxville

Kyle Everett Anderson

August 2020

Acknowledgments

I would first like to thank Dr. Steven Skutnik, Dr. Ondřej Chvála, and Alex Wheeler who I have worked closely with over the past two years on this project. As my advisor Dr. Skutnik has provided extensive guidance and help with this work. He has driven me to improve on many portions of this work and to improve on my scientific and engineering skills more generally. I am graduate for the advice and help Dr. Chvála has given me on this work, especially related to molten salt reactors and to the use of the high-performance cluster. I am especially thankful to Alex Wheeler whom I have had countless discussions about this work with, his deep knowledge of molten salt reactors and willingness to share it has been immensely helpful.

I am exceedingly thankful for others who have this work possible, both at UT and elsewhere. I am grateful to Dr. Ivan Maldonado for being both a wonderful teacher and for serving as a member of my committee. I am also grateful for support through the NRC fellowship program and the DOE NEUP program. Finally, I would like to express my appreciation for my friends, family, and partner who have given me unending support throughout the past two years.

Abstract

This thesis details the generation of ORIGEN reactor libraries for liquid-fueled molten salt reactors. ORIGEN reactor libraries are a useful tool to quickly calculate the isotopic source term of a reactor. These libraries have been extensively studied and used for traditional reactor types, however, are not available for molten salt reactors. This thesis presents work on generating these libraries for molten salt reactor designs, including those with fission product processing and online refueling. Libraries for a single-fluid thermal fluoride salt reactor were created using the SCALE code system. These libraries were spaced using a new methodology based on analyzing the transition matrices of the libraries themselves. Additional libraries were generated that included the removal of fission products from the reactor. A methodology based on the effective one-group removal cross section of fission products was developed to limit the number of libraries needed to correctly capture the effects of fission product removal. Finally, a set of libraries was created that contained online refueling with varying feed rates and enrichments. This work created a robust method for generating ORIGEN reactor libraries for a variety of molten salt reactor designs. Additionally, it showed that the inclusion of advanced design features, such as fission product processing and online refueling, in the libraries is possible.

Table of Contents

List of Tables

List of Figures

Chapter 1

Introduction

The impetus behind the work in this thesis is a larger project to develop a software framework for testing material control and accounting (MC&A) methods on liquid fueled molten salt reactors (MSRs). A key component of this framework is developing a reactor physics module that is capable of quickly simulating the isotopics of a large number of MSR designs. One possible approach is to use pre-generated cross-section libraries to perform point depletion calculations, such as is possible using ORIGEN reactor libraries.

ORIGEN reactor libraries have been studied and used extensively for commercial reactor designs. However, they have not been developed for liquid-fueled molten salt reactors. This thesis describes the generation of these reactor libraries over six chapters, including a background chapter, three chapters of analysis, and an introduction and conclusion chapter.

The background chapter gives an overview of the core characteristics of MSRs that are relevant to nuclear MC&A. This includes discussion of the design space of MSRs and how the choice of neutron spectrum, salt type, fluid number, fuel composition, and conversion factor effect properties relevant to MC&A. Additionally, background on various salt processing systems is given.

The three chapters of analysis focus on the development of ORIGEN reactor libraries for MSRs. The first of these chapters describes the creation and spacing of libraries for a thermal single-fluid uranium-fueled reactor. A new methodology is for spacing the libraries is detailed and tested. The second chapter focusing on including fission product removal in the ORIGEN reactor libraries. Two types of fission product removal are studied and new a

methodology is tested for limiting the number of libraries needed to model fission product removal. The final chapter focuses on incorporating online refueling into the libraries at various feed rates.

Chapter 2

Core Characteristics Relevant to Material Control and Accounting in Liquid-Fueled Molten Salt Reactors

2.1 Introduction

The term molten salt reactor covers a wide range of nuclear reactor designs that utilize molten salts as a coolant or both a coolant and a fuel carrier. MSRs vary in the composition of salt used, the neutron spectrum of the core, and the fuel form, among other properties. In general, MSRs are operated at high temperatures and low pressures, opposite to the current fleet of light water reactor designs. The term "MSR" in this thesis will refer exclusively to liquid-fueled MSRs. While other salt-cooled reactor designs exist (where the fuel is in a solid form and salt acts solely as a coolant, such as the Fluoride High Temperature Reactors or FHRs [20]) in terms of safeguards these reactors are more akin to other solid fuel reactors; this is especially true for designs such as High Temperature Gas Reactors, in which the fuel is a discrete countable object.

The characteristics of liquid fueled molten salt reactors (MSRs) present new challenges for material control and accounting (MC&A). Unlike the current fleet of nuclear reactors, the nuclear material in MSRs cannot be item-counted. Instead of fuel being in discrete

physical units, the fuel of an MSR is dissolved in a continuously flowing liquid that changes properties over time. In addition to the fuel, nuclear material is often in a gaseous, liquid, or solid form throughout the reprocessing system of the reactor. This chapter gives an overview of MSR properties and their relevance to MC&A. The first section gives an overview of the vast design space of MSRs that includes differences in neutron spectrum, salt choice, fluid number, fuel composition, and conversion factor. The second section gives an overview of the various methods of salt processing available for MSR designs.

2.2 Fuel Cycle Design Space of Molten Salt Reactors

The overall design space of molten salt reactors is vast with various choices for major reactor characteristics. Table 2.1 shows some potential choices for major reactor characteristics. These design characteristics are interconnected to one another in varying degrees and a change in any one of them will have significant ramifications for material control and accounting.

Table 2.2 lists the design characteristics of MSRs listed in the International Atomic Energy Agency's Advanced Reactors Information System (ARIS) database. This table is not fully comprehensive of all MSR designs currently being developed but does give insight into a large number of them. The table highlights the vast number of choices of the parameters as well as the interconnectedness of the parameters.

Table 2.1: Potential design choices for given reactor characteristic

Reactor Characteristic	**Possible Design Choices**
Neutron Spectrum	Thermal, Fast, Varying
Salt Choice	Fluoride, Chloride
Fluid Number	Single, Dual
Fuel Composition	U, Pu, SNF
Conversion Factor	Breeder, Burner

Table 2.2: Design Characteristics of MSRs in the ARIS database [11].

Reactor	Design Characteristics				
	Spectrum	**Salt Choice**	**Fluid Number**	**Fuel Composition**	**Conversion Factor**
IMSR-400	Thermal	Fluoride	Single	U-235/Pu	Burner
LTFR	Thermal	Fluoride	Dual	U-233	Breeder
MSFR	Fast	Fluoride	Dual	U-233/U-235/Pu	Breeder
MSR-FUJI	Thermal	Fluoride	Single	U-233	Breeder
MSTW	Thermal	Fluoride	Single	SNF	Burner
SSR-U	Thermal	Fluoride	Single	U-235/Pu	Burner
ThorCon	Thermal	Fluoride	Single	U-235/Pu	Burner

To understand the effect of each of these design characteristics on MC&A they are individually detailed in the following sections.

2.2.1 Neutron Spectrum

Molten salt reactors designs have neutron spectra ranging from fast to thermal. The neutron spectrum characterizes the energy of neutrons inside a reactor driving the majority of fission events. There is no single definition of the energy ranges, however most are similar to the following defined by the International Atomic Energy Agency where the spectrum is broken into three regions: the thermal region (neutron energies up to 0.5 eV), the intermediate region (neutron energies from 0.5 eV to 0.1 MeV), and the fast region (neutron energies above 0.1 MeV) [9].

Since fission neutrons are born at fast speeds a moderator must be used to achieve a thermal spectrum. Most thermal MSR designs utilize a large volume of graphite as a moderator (See ARIS database). Other moderators such as beryllium oxide or zirconium hydride have been used in thermal designs [2] [23]. In a fast spectrum MSR a moderator is not used, and instead fast neutrons are used to sustain the reaction.

The neutron spectrum of an MSR will heavily influence reactor properties relevant to MC&A, including: the choice of salt, the reactor conversion factor, and the amount of startup fissile material. Generally, a thermal spectrum design will use a fluoride salt (See Section 2.2.2), have a lower reproduction factor than a fast spectrum design (See Section 2.2.5), and have less startup fissile material than a fast spectrum design.

The difference in the needed amount of startup fissile material is driven by changes in fission cross-sections at different neutron energies. The fission cross-sections for the fissile isotopes U-233, U-235, and Pu-239 are approximately one hundred times greater in the thermal spectrum than the fast spectrum. However, the fission-to-capture ratio is lower in the fast spectrum compared to the thermal spectrum (this does allow for higher actinides to be efficiently processed). Overall, the difference in cross-sections allows for a thermal spectrum reactor to be run with less fissile material [28]. The amount of fissile material used to startup a reactor is important to MC&A as it will determine how much material needs to be initially accounted for.

2.2.2 Salt Choice

In a liquid-fueled MSR, the salt must have the proper physical properties to act both as a coolant and a fuel carrier. An ideal coolant should have the following properties: low vapor pressure (and consequently, a high boiling point) so that coolant will have a lower tendency to vaporize; a high specific heat and high density at operating pressures so that a large amount of energy can be transferred to the coolant; a high thermal conductivity so that energy can be more readily transferred from the coolant [19]. Meanwhile, an ideal fuel carrier be able to perform all of the following functions: ability to dissolve more than the critical concentration of the fissile material, dissolve all fission products without losing the salts other relevant properties, and be able to survive fission events that lead to complex speciation in the salt from ionized fission products [25]. An additional requirement of the salt is that it must be chemically compatible with the reactor materials it comes in contact with.

The majority of MSR designs utilize fluoride salts while a few designs use chloride salts. Other candidate salts are ruled out for a variety of reasons. Metal halide salts and oxygen

containing salts are too corrosive at operational temperatures to be practical for reactor-based applications. In addition to their corrosiveness, oxides have a high melting point and nitrates have lower stability in high radiation fields [26]. Heavy halide salts have inferior thermophysical properties compared to fluoride and chloride salts and are more expensive than these salts. Mixed halide salts are more complicated to create and do not offer any notable advantages over fluoride or chloride salts.

The choice of salt is further narrowed by the choice of neutron spectrum. In a thermal spectrum, fluoride salts are attractive because of the low absorption cross-section of fluorine. In a fast spectrum reactor designs, chloride salt is often used as it has a lower moderating power than fluoride salts; however fluoride salts are nonetheless viable and suitable for a burner reactor because of their high actinide solubility [3].

The composition of the salt has a large effect on the short-term activation of the salt. The production of relatively long-lived isotopes (on the order of days) that are strong gamma emitters is a concern. These isotopes will cause the salt to have a high activity with gammas that can penetrate through structural materials. Specifically, the production of K-42 and from Na-24 via activation of potassium and sodium is a concern for a few days after their production. Both rubidium and zirconium have several activation products with high energy gammas that have half lives on the order of weeks. If it is preferred to have reprocessing and refueling to be a continuous process then salts containing these constituents will have to undergo remote reprocessing and refueling. Otherwise salts with these constituents could be left to decay and then processed in batch.

2.2.3 Fluid Number

The fuel salt in a MSR can be located in a single region or in two separate regions. The separation of salt into two regions is done to allow for separate regions for breeding and burning. A MSR with one region is classified as a single-fluid reactor, while a MSR with two regions is classified as a dual-fluid reactor.

In a single-fluid reactor the core is comprised of a single region with salt containing the fissile material. There is no separate blanket area for breeding. The fertile material is included as an integral component of the fuel salt if the reactor is being run as a breeder (i.e.,

creating more fissile material than it is consuming). The Molten Salt Reactor Experiment was a single fluid MSR [18]. A major advantage of single-fluid MSR is their design simplicity.

By contrast, a two-fluid MSR consists of a core area with fissile material is surrounded by a blanket of fertile material. The core area sustains a chain reaction and continuously leaks neutrons in the blanket region. These neutrons are captured by fertile material in the blanket and converted into fissile material. Some configurations of the Molten Salt Actinide Recycler & Transmuter are examples of two-fluid reactor [15]. The principal advantage of the two-fluid design is a simplicity of the thorium fuel cycle implementation.

A two-fluid MSR has some operational advantages compared to a single fluid MSR. Since there are minimal fission products in the blanket salt, the processing of fissile material easier than a single fluid MSR. Uranium can be oxidized to a hexavalent state, while thorium stays tetravalent, which simplifies processing design for the thorium fuel cycle. Additionally, neutron losses in the blanket region are minimized by the dilution of parasitic isotopes in the large blanket region [13]. However, the two-fluid MSRs provide additional challenges for MC&A. Nuclear material in these reactors must be accounted for in two different systems which are partially connected and have material moving between them.

2.2.4 Fuel Composition

The fuel composition of molten salt reactors varies greatly design-to-design. The most major difference between designs is the choice of a thorium, uranium, or mixed fuel cycle. The choice in fuel cycle will determine the major fissile isotopes within the reactor and thus greatly impact material control and accounting. Therefore, it is important to understand the different possible fuel loading of MSRs.

The thorium fuel cycle can be implemented in either an open or closed fashion in a molten salt reactor. In the open fuel cycle, Th-232 is mixed with low enriched uranium (LEU), or other fissile, to fuel the reactor. At the start of the cycle the U-235 from the LEU provides all of the power. As the Th-232 is transmuted the source of power changes from U-235 to U-233. The isotope U-233 does not occur naturally, and instead is bred from thorium. Natural thorium is composed almost entirely of Th-232 (99.98%). After the cycle is complete the fuel salt is disposed of and no fissile materials are recovered from used fuel salt [10].

The closed fuel cycle begins in the same fashion as the open cycle, with a mixture of Th-232 and some fissile fuel to start the reactor. However, in the closed cycle the fuel salt is processed during the reactor operations. As the salt is processed, fission products and protactinium are removed from the salt. Protactinium is allowed to decay to U-233 which is then mixed with Th-232 to form new fuel that continues to power the reactor after startup. No additional U-235 is needed after the initial startup. In a two-fluid system, the bred uranium can be separated instead or along with protactinium, and the thorium and uranium are not mixed since the thorium blanket and uranium core are separate fluids.

The material attractiveness of the uranium for diversion can be decreased by adding U-238 to the U-233 bearing salt. To denature the uranium, a ratio of around six to one U-238 to U-233 would be added to the fuel salt after reprocessing had taken place. The denaturation process would make uranium unusable for weapons purposes without isotopic separation [4]. Although denaturing would eliminate some of the proliferation risk from uranium, it would add risk from plutonium. U-238 is fertile and can be transmuted to Pu-239 through neutron capture. This plutonium would then have to be tracked throughout the system in addition to uranium.

If the reprocessing of the fuel salt occurs, protactinium will be separated out and allowed to decay to uranium. The two short-lived isotopes Pa-232 and Pa-233 are generated from a series of neutron captures and beta decays in thorium and are of interest in safeguards protection. Pa-233 decays to U-233 via beta decay with a half-life of 27 days and Pa-232 decays via beta decay to U-232 with a half-live of 31 hours. U-232 has multiple daughter isotopes that emit high-energy gammas, including a 2.6 MeV gamma from Tl-208 [27]. U-233 is generated in much higher quantity than U-232. The difference in half-lives of the two protactinium isotopes presents a challenge for safeguarding against the diversion of U-233 [7]. If all of the isotopes were left to decay for 15 days, nearly all of the Pa-232 will have decayed to U-232. This uranium could then be processed out of the mixture leaving pure Pa-233 to decay to U-233.

The uranium fuel cycle in an MSR can also be run in either an open or closed fashion. The reactor itself can be utilized as a burner or breeder with either a thermal or fast spectrum

[8]. A uranium fuel cycle in an MSR is more closely related to the current fuel cycle of light water reactors around the world.

This fuel cycle relies on LEU fuel, meaning it is a mixture of U-238 and U-235 with less than 20% of the U-235 isotope. At the start of the cycle the U-235 sustains the nuclear reaction. Throughout the cycle Pu-239 will be breed from the U-238 in the fuel. The conversion occurs due to neutron capture by U-238 and subsequent beta decays. The bred plutonium contributes to the chain reaction in increasing amounts as the cycle progresses. The breeding of plutonium presents challenges for safeguards. In a MSR running on a uranium fuel cycle, both the uranium and plutonium must be tracked. These challenges have similar parallels to a denatured thorium-uranium fuel cycle.

2.2.5 Conversion Factor

The conversion factor of a reactor is the ratio of the amount of fissile material consumed to the amount of fissile material produced. If the conversion factor is greater than one, the reactor is considered a breeder, in that it creates more fuel than it consumes. The conversion factor of a reactor is derived from the reproduction factor of the fuel. The reproduction factor is a measure of many neutrons are produced from fission per how many neutrons are absorbed in the fuel, as shown in Equation 2.1, where η is the reproduction factor, ν is the average number of neutrons per fission, Σ_f is the fission cross-section, and Σ_c is the capture cross-section.

$$\eta = \frac{\nu\Sigma_f}{\Sigma_f + \Sigma_c} \tag{2.1}$$

If the reproduction is above two then breeding of additional fuel is possible. In this case one neutron is used to sustain the chain reaction and the excess neutron is used to breed new fuel from fertile material. This factor is dependent on neutron energy and changes significantly from thermal to fast spectrum. Table 2.3 shows reproduction factors for fissile isotopes U-233, U-235, Pu-239 in both thermal and fast neutron spectrum energies.

Table 2.3: Reproduction factor (η) for select fissile isotopes in thermal and fast neutron spectrum MSRs [14].

Isotope	Thermal Spectrum	Fast Spectrum
U-233	2.29	2.56
U-235	2.07	2.38
Pu-239	2.12	3.10

The reproduction factor of U-235 and Pu-239 is just above 2 at thermal energies, while U-233 is closer to 2.3. The two thermal spectrum breeder reactors listed in the ARIS database (Table 2.2) are U-233 fueled reactors. The reproduction factor in the fast spectrum is higher for all three isotopes with Pu-239 the highest at 3.1. The single fast spectrum reactor listed in the ARIS database is a breeder reactor with a proposed fuel of U-233, U-235, or plutonium.

2.3 Salt Processing Systems

The majority of MSRs designs include some combination of salt processing systems. Salt processing can range from simple fission product processing systems to complex online refueling systems. The removal of fission products allows for many benefits, including: improved neutronics performance, the reduction of the reactor's core accident source term, and the removal of corrosion inducing elements. Online refueling gives design benefits such as, continuous operation, a limited amount of excess reactivity in the core, and a larger number of fuel cycle choices, among others.

There are many viable salt processing techniques available for molten salt fuel that can be used separately or in various combinations. The main techniques include: electrochemical separation, fluoride salt volatilization, gas extraction, liquid metal extraction, and vacuum distillation. The following sections give a brief overview of each technique summarized from information from *Molten Salt Reactors and Thorium Energy* [24].

2.3.1 Gas Extraction

The gas extraction process, also known as sparging or bubbling, utilizes an inert gas to remove dissolved neutron poisons from the system. The process has been used in practice in the MSRE, where both helium and argon were used successfully to remove xenon and krypton from the system. The gas extraction process can be understood through Henry's Law for partial pressures. The law states the amount of dissolved gas in a liquid is proportional to the partial pressure of the gas in the volume around the liquid. If inert gases are added to the liquid, differences in partial pressures will drive other gases out of the liquid.

The gas extraction process removes additional non-gaseous fission products from the molten salt. At MSR operating conditions, many elements such as niobium, molybdenum, ruthenium, antimony, and tellurium do not form stable fluoride compounds within the salt. These suspended particles are removed from the salt with gas extraction process and settle as dust in the off-gas system. At the operating conditions where helium bubbling is performed, protactinium, uranium, and plutonium should be soluble in the salt and not removed from the salt by bubbling.

2.3.2 Electrochemical Separation

In electrochemical separation, specific lanthanides and actinides (which dissolve in the salts), are separated from the salt using electrochemical reactions. To achieve the separation electrodes are placed in the salt, which acts as an electrolyte. A voltage is applied to electrodes and elements plate out on the working electrode by electromotive force.

Which elements are able to be separated out of the salt depended on the electrochemical stability of the salt. Each individual salt mixture has unique redox potentials for each lanthanide and actinide.

2.3.3 Fused Salt Volatilization

Fused salt volatilization, or fluoride volatility, is a process based on the chemical reaction of fluorine gas with elements dissolved in the fluoride molten salt. Fluorine gas is bubbled

through the molten salt, dissolved elements in the salt form volatile fluorides when the gas is passed through the salt. The fluorides are then processed out the salt.

The fluorination process is run in a temperature range of 500-550°C and can be run as a continuous process. Most notability, the process removes uranium from the molten salt carrier where the dissolved uranium is transformed into UF_6. Multiple dissolved fission products will also form volatile fluorides that can be removed, including cesium, chromium, niobium, molybdenum, ruthenium, and tellurium. These fission products volatiles are trapped in a sorption system while the uranium hexafluoride is trapped in a cold trap where it can be extracted.

For material accountability purposes, the concentration of uranium in the fuel salt needs to be known before and after the fluorination process. The concentration difference in the fuel salt combined with the volumetric flow rate can be compared against the amount of hexafluoride in the cold trap.

2.3.4 Liquid Metal Extraction

Liquid metal extraction can be used to remove fission products from the molten salts. The process relies on reductive extraction reactions which are generally described in Equation 2.2 [5].

$$MX_a + (a/b)R = M + (a/b)RX_b \tag{2.2}$$

Depending on the given salt, salt impurities, and metal reductant: M represents a lanthanide or actinide, X chlorine or fluorine, and R the metal reductant. a/b represents the coefficient in the chemical equation. MX_a and RX_b are dissolved in the molten salt, while R and M are dissolved in the liquid metal.

This method was studied with bismuth as the metal reductant during the MSRE era. Bismuth was chosen for its low melting point, small vapor pressure at MSR operating temperatures, and because it does not dissolve into fluoride or chloride salts. The disadvantage of bismuth is the large difference in mass density compared to the fuel salts, which results in less efficient mixing.

The liquid metal extraction process can remove both protactinium and uranium from the salt. The process can be placed after a fused salt volatilization process so that only protactinium is removed in the process. Throughout this process the protactinium is continuously decaying into uranium.

2.3.5 Vacuum Distillation

Vacuum distillation is a well-known process to separate the individual components of a mixture. In a given mixture the individual components may have different volatilities. This difference in volatility can be used to selectively boil off and separate the components. Performing distillation under reduced pressure - near vacuum - reduces the boiling points of the components, thus the process can be done at lower temperatures.

Vacuum distillation could be used to remove fission products from the carrier salt in an MSR system. Laboratory scale tests showed decontamination factors for rare earths fission products ranging from 100 to 1000 [21]. Relatively few studies of vacuum distillation for MSRs have been done. In a fully operational reprocessing system the vacuum distillation technique would likely be combined with fused salt volatilization.

Chapter 3

Generation of ORIGEN Reactor Libraries for Liquid Fueled Molten Salt Reactors

3.1 ORIGEN Reactor Libraries

The ORIGEN code calculates nuclide generation, depletion, and decay in a system by solving a set of ordinary differential equations of the same form as Eq. 3.1 [17].

$$\frac{dN_i}{dt} = \sum_{j \neq i} (l_{ij}\lambda_j + f_{ij}\sigma_j\phi)N_j(t) - (\lambda_i + \sigma_i\phi)N_i(t) + S_i(t), \tag{3.1}$$

where,

N_i = Number of nuclide i

λ_i = Decay constant of nuclide i

l_{ij} = Fraction yield of nuclide i from decay of nuclide j

σ_i = Removal cross-section for nuclide i

f_{ij} = Fraction yield of nuclide i from neutron-induced removal of nuclide j

ϕ = Angle and energy-integrated time-dependent neutron flux

S_i = Time-dependent source/feed of nuclide i

The set of equations can be simplified into the matrix form of Eq. 3.2 where A is termed the transition matrix.

$$\frac{d\vec{N}(t)}{dt} = \mathbf{A}\vec{N}(t) + \vec{S}(t) \tag{3.2}$$

ORIGEN can be run in many different manners, including as part of a larger coupled calculation or as a standalone calculation. One such way to run a standalone calculation is to use ORIGEN reactor libraries. These libraries are sets of burnup-dependent, one-group point cross-sections. By using these libraries ORIGEN is able to quickly calculate the nuclide concentrations in a system over time. When using these libraries, a flux or power is provided by the user and decay coefficients are generated from internal ORIGEN data.

The most innate way to create an ORIGEN reactor library is through a coupled neutron transport and depletion calculation. During this calculation, cross-section data is collapsed across both space and energy to solve the updated depletion step. This collapsed cross-section data is then saved into a reactor library.

Libraries generated in this manner are not profusely useful for carrying out point depletion calculations as a depletion solution already exists from the coupled transport calculation. Therefore, a more functional way to use ORIGEN reactor libraries is through interpolation. By interpolating libraries over problem-dependent conditions (such as initial enrichment, burnup, etc.), approximate cross-section data can be generated at new parameter points without the need for a coupled transport calculation. When done correctly, interpolation allows for calculating approximate reactor isotopics with little computational expense.

Historically, the Automatic Rapid Processing (ARP) code has been used to interpolate over ORIGEN reactor libraries. In this code interpolation schemes were generated for specific reactor types by analyzing the changes in cross-sections versus various reactor parameters, e.g., enrichment, burnup, water density [12]. A major constraint with the ARP methodology is the inability to interpolate over reactor parameters not already included. This constraint was addressed by a more recent code using generalized N-dimensional interpolation, styled OBIWAN [22].

In this code any number (N) of generic parameters can be tagged to ORIGEN libraries. This tag includes the name of the parameter and the value of the parameter to use in interpolation. A user can then choose a point in this N-dimensional parameter space for interpolation. The libraries closest to this chosen point are interpolated over to generate a new library. For all parameters other than burnup a linear interpolation is used.

Many sets of ORIGEN reactor libraries have been generated and are included in the SCALE code system. There are a large variety of reactor systems available spanning different coolants, fuels, and moderator types. However, there is currently no available sets of libraries for MSRs. This chapter lays out a methodology for creating sets of ORIGEN reactor libraries for MSRs and includes results from a set of libraries for single-fluid thermal fluoride salt reactors.

3.2 Single-Fluid Thermal Fluoride Salt Reactor

The design space for MSRs is extremely large as noted in Chapter 2. Therefore, it is useful to breakdown the design space of reactor libraries into two groups, immutable and mutable design parameters. Immutable design parameters encompass large scale design choices that are not easily changed such as, fluid-number, salt type, spectrum, etc. Mutable design parameters would include design choices that are easily varied such as enrichment or reactor geometry.

In the case of ORIGEN reactor libraries, a single set of libraries would be composed of all the same immutable design parameters. However, multiple libraries would be available for calculating designs at any mutable parameter through interpolation. For the first set of reactor libraries, a single-fluid thermal-spectrum fluoride salt reactor was chosen. This was determined to be a natural starting point based on the large amount of research that has been done on single-fluid thermal fluoride salt reactors, including the notable Molten Salt Reactor Experiment [6].

It is not feasible to include every mutable design parameter within a set of libraries. Therefore, a determination must be made of which parameters to include and how to space these parameters within in the library set. For existing reactor types the determination of

which parameters to include is normally determined by what experimental validation data exists for the reactor type. However, in the case of MSRs there is no extensive validation data available. Therefore, the decision on what parameters to include must be decided another way.

In theory any parameter would be valid to add to the design space if it had a discernible effect on reactor neutronics and fuel depletion when varied. However, there are a large number of parameters that meet this criteria and overall the number of parameters should be minimized as much as possible. This is because the number libraries as well as the computational resources to generate and store them, grow exponentially compared to the number of parameters included. It is not possible to determine which parameters have the largest effect on reactor neutronics and fuel depletion a priori. Therefore, which parameters to include were based on a combination of limited analysis and engineering judgment.

A study on thermal fluoride MSR lattice optimization was used as a starting point for choosing parameters [16]. This studied shows there is a significant effect on the reactor neutronics based on varying the lattice pitch and salt fraction (the fractional volume of the fuel channel that contains the fuel salt) in a thermal fluoride MSRs. Fuel enrichment was included as a parameter based on the end use of the libraries for material control and accounting. The reactor core size was included as a parameter after limited analysis showed that its variation had an effect on reactor neutronics (this variation can be fully seen in Section 3.3). An upper-bound of four meters was placed on the core diameter.

Table 3.1 shows the parameters and their initial spacing for the single-fluid thermal fluoride salt reactor model. The model represents a graphite-moderated system with fuel channels arranged in a hexagonal pitch array with a variable radial dimension. The model has a varying number of rings of fuel channels surrounding the center of the core. A downcomer region of salt, a graphite reflector, and a steel vessel wall surround the core. A gas region surrounds the core to create a square geometry as a circular geometry cannot be solved using the SCALE transport solver NEWT.

Table 3.1: Parameter Space for Single-Fluid Thermal Fluoride Salt Reactor

Parameter	Range	Spacing
Enrichment [wt. % U-235]	2-10	1
Lattice Pitch [cm]	10-50	10
Salt Fraction [-]	0.1-0.5	0.1
Fuel Channels Rings [-]	1-7	1

Table 3.2 shows the remaining attributes for the model and Figure 3.1 shows an example geometry of one of the models. The MSR lattice optimization study was used as a starting point for deciding the model attributes [16]. The attributes were chosen permissively and do not represent any particular MSR design as the attributes would almost certainly change over the range of parameters chosen. Python scripts were created to generate all of the variations of the model and were run in SCALE 6.2.3 using the TRITON/NEWT sequence. The scripts were built to easily allow variation of any of the parameters or model attributes if others need to generate libraries with different parameter/attribute values. More information about these scripts can be found in Appendix A.

3.3 Transition Matrix Spacing Methodology

An important component in creating new sets of reactor libraries is to determine the ideal spacing of the mutable parameters chosen. As previously mentioned, the spacing of reactor libraries is normally done by analyzing the change in cross-sections for select isotopes. Instead of adapting this methodology for MSRs, a new methodology was created and tested using analysis of the transition matrices. In this methodology the parameter spacings which minimize the error in actinide mass from interpolation are calculated using the actinide transition coefficients.

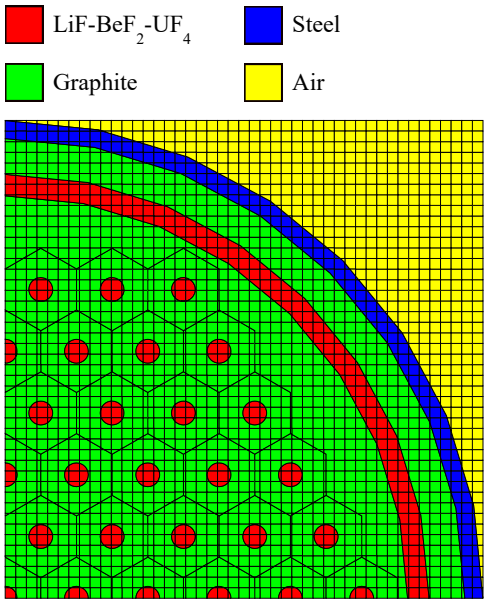

Figure 3.1: Example geometry of the Single-Fluid Thermal Fluoride Salt Reactor generated from NEWT including the mesh overlay.

Table 3.2: Additional Single-Fluid Thermal Fluoride Model Attributes

Attribute	**Value**
Power	20 MW
Salt Temperature	923 K
Salt Density	3.353 g/cm^3
Li-7 Enrichment	99.995 %
Graphite Temperature	950 K
Graphite Boron Concentration	1.503 ppm
Downcomer Thickness	3 cm
Reflector Thickness	5 cm
Vessel Wall Thickness	2.5 cm
Cycle Length	3000 Days
Fuel Loading	1 MTHM

Interpolation of the ORIGEN reactor libraries is done using the transition matrix coefficients of the libraries. The transition matrix also governs the amount of nuclides in the system and therefore the error in isotope masses from interpolation. Computing the error outright is not trivial as the solution for the isotope masses includes a matrix exponential as shown in Equation 3.3. The solution for a single isotope requires the successive multiplications of terms in the transition matrix as shown in Equation 3.4 and thus is not trivial to compute either [17].

$$\vec{N}(t) = exp(\mathbf{A}t)\vec{N}(0) = \left(\sum_{k=0}^{\infty} \frac{(\mathbf{A}t)^k}{k!}\right)\vec{N}(0) \tag{3.3}$$

$$\begin{aligned} N_i(t) = N_i(0) + t\sum_j a_{ij}N_j(0) + \frac{t}{2}\sum_k \left[a_{ik}t\sum_j N_j(0)\right] + \\ \frac{t}{3}\sum_m \left(a_{im}\frac{t}{2}\sum_k \left[a_{mk}t\sum_j a_{kj}N_k(0)\right]\right) + ... \end{aligned} \tag{3.4}$$

Although computing the exact solution to the error is challenging computing an approximate proportionally to the error should be simpler. In this case the solution is first narrowed down to the first-order rate coefficients. This would mean the solution to any isotope would be as shown in Equation 3.5.

$$N_i(t) = N_i(0) + t\sum_j a_{ij}N_j(0) \tag{3.5}$$

where,

$$a_{ij} = \begin{cases} l_{ij}\lambda_j + f_{ij}\sigma_j\phi & i \neq j \\ -\lambda_i - \sigma_i\phi & i = j \end{cases}$$

If the difference in initial mass values is assumed negligible then the error between libraries will be approximately proportional to the difference in the first-order rate coefficients.

3.3.1 Transition Matrix Analysis

This methodology was tested using the single-fluid thermal fluoride salt reactor libraries. The difference in the reaction portion of the transition matrix values were calculated on an absolute basis for all actinide reactions and then averaged as shown in Equation 3.6, where n_i is the number of actinide isotopes, A is the set of all actinides in the system, R_p is the set of all reactions leading to the production of an isotope, R_l is the set of all reactions leading to the loss of an isotope, $\sigma_{i,r}$ is the cross-section for reaction r with isotope i, and f_{ir} is the fractional yield of the nuclide i from reaction r.

$$\Delta\overline{\overline{A}} = \frac{1}{2}\left(\frac{1}{n_i}\sum_{i\in A}\left|\sum_{r\in R_p} f_{ir}\sigma_{i,r} - \sum_{r\in R_p} f_{ir}\sigma'_{i,r}\right|\right) + \left(\frac{1}{n_i}\sum_{i\in A}\left|\sum_{r\in R_l} \sigma_{i,r} - \sum_{r\in R_l} \sigma'_{i,r}\right|\right) \tag{3.6}$$

These values were then used to find the optimal spacing for the parameters by minimizing the difference in transition matrix values. Additionally, the actual error in actinide mass from interpolation was calculated using ORIGEN. This was done to validate the transition matrix spacing methodology and to give an error value on the spacings. The error was calculated as the averaged percent difference of the select isotopes shown in Table 3.3. A percent difference error is used as otherwise the difference in U-238 mass will dominate the solution. Only a select number of isotopes are used for the error calculation because isotopes with extremely small masses can have large percent errors from only a small absolute difference in mass. The selected isotopes were chosen by including any actinides who mass represented greater than 1% of all actinides other than U-235 and U-238.

Table 3.3: Select Isotopes for Determining Average Error

Select Isotopes			
U-235	U-236	U-238	Pu-239
Pu-240	Pu-241	Np-237	Np-239

Figures 3.2a, 3.3a, 3.4a, and 3.5a show the absolute difference in transition matrix values between libraries within a single parameter. The difference in transition matrix values was calculated relative to the lowest parameter value. All other parameters are constant when the difference in transition matrix values are calculated. Additionally, a color map corresponding to burnup is overlaid on the points. Each parameter has both a unique range and distribution of values for the difference in transition matrix values. The salt fraction parameter has the largest range of values while the uranium enrichment parameters has the smallest range of values. The stratification of burnup points in the figures shows that the parameters are not fully independent of one another.

The difference in transition matrix values for the salt fraction and lattice radius parameters always significantly increases as the parameter values are increased. However, the difference in transition matrix values for the number of fuel rings parameters does not always significantly increase as the parameter values are increased. This suggests that a change in the salt fraction and lattice radius will always have a significant effect on the system while a change in the number of fuel rings may not. For low burnup values an increase in the uranium enrichment parameter changes the difference in transition matrix values significantly, however, this is not seen at higher burnup values. This suggests that the system is more sensitive to the initial uranium enrichment in the early portions of the cycle compared to the later portions.

Figures 3.2b - 3.5b show the correlation between the difference in transition matrix values and the error in actinide mass between interpolated and generated reactor libraries. For all four of the parameters there is a weak correlation between the mass error and difference in transition matrix values. For the uranium enrichment parameter only half of the libraries were used to generate the correlation because of the large amount of computational resources needed for a calculation using all the libraries.

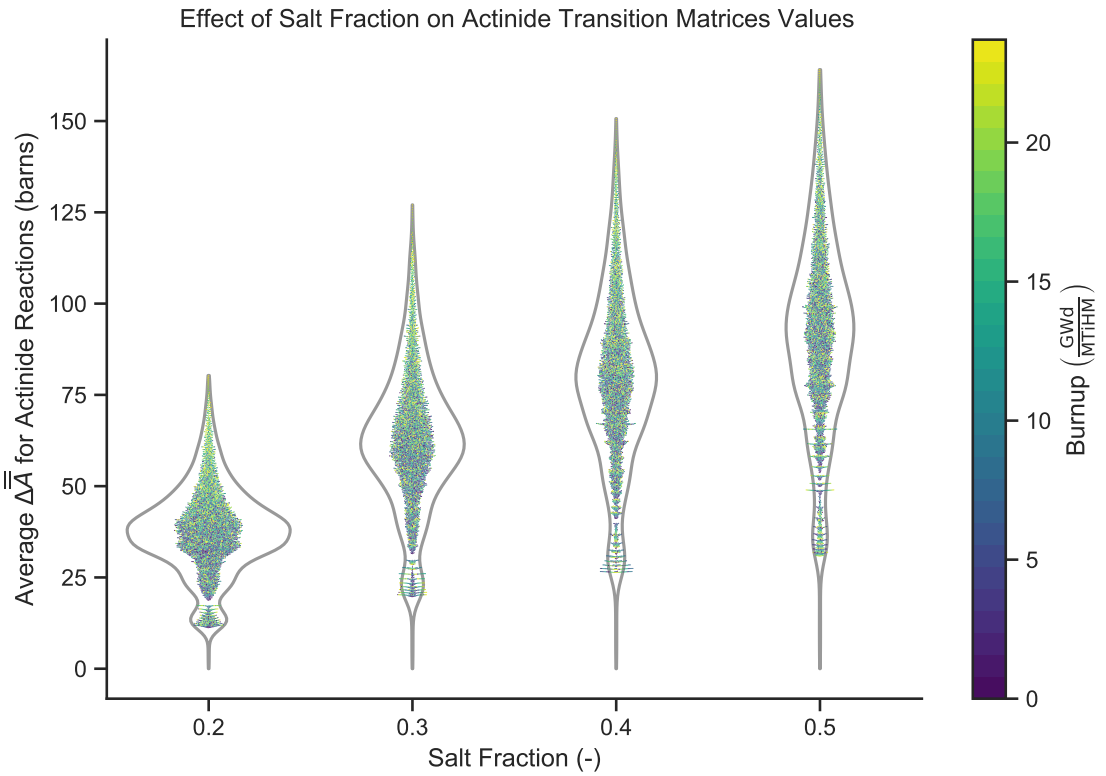

(a) The average difference in transition matrix values compared to libraries with a salt fraction of 0.1 (-).

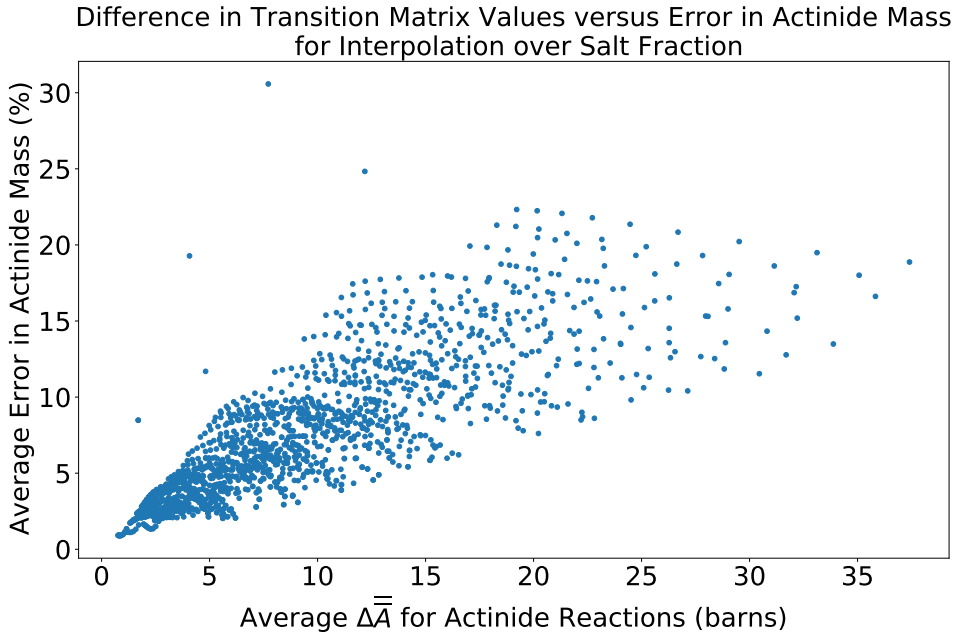

(b) The difference in transition matrix values versus error in actinide mass for interpolating over salt fraction for all single spacing possibilities.

Figure 3.2: Salt Fraction Transition Matrix Analysis

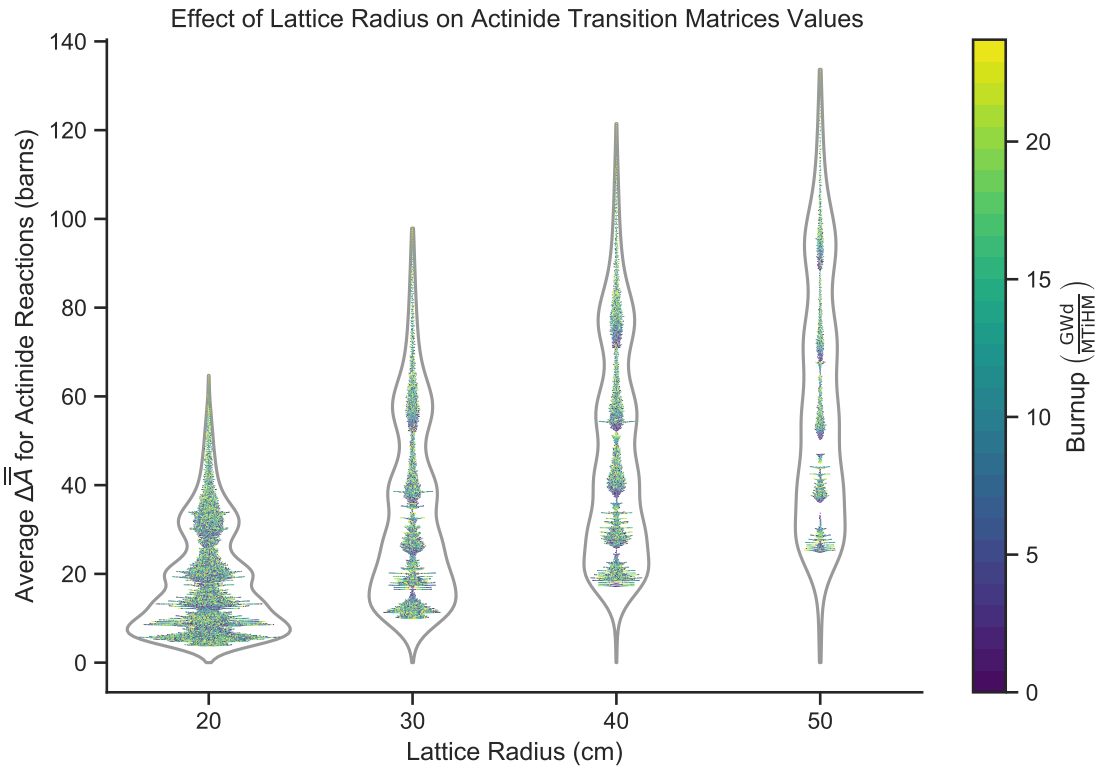

(a) The average difference in transition matrix values compared to 10 (cm) lattice radius libraries.

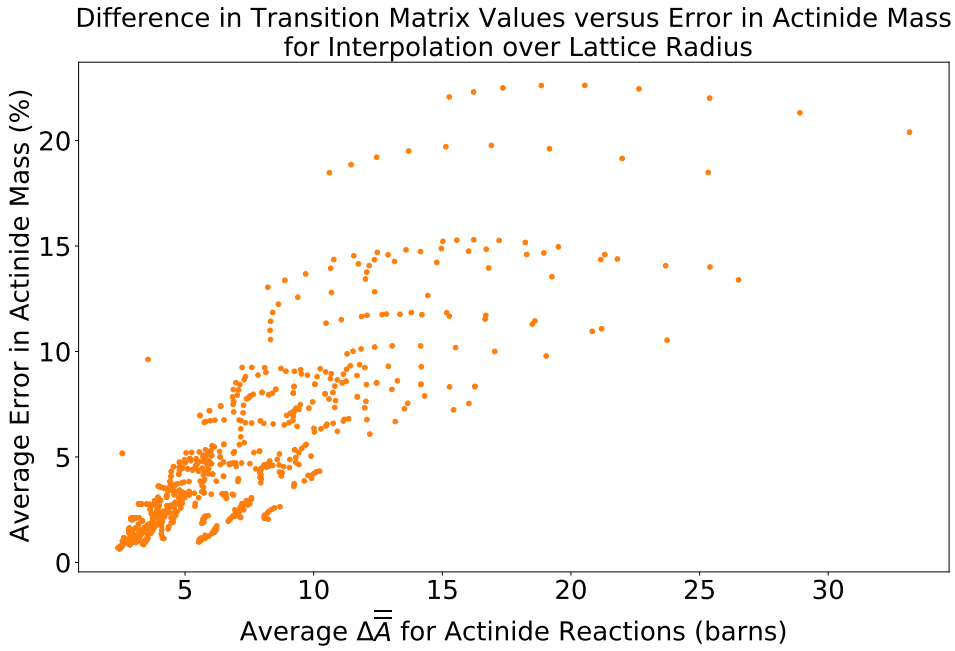

(b) The difference in transition matrix values versus error in actinide mass for interpolating over lattice radius for all single spacing possibilities.

Figure 3.3: Lattice Transition Matrix Analysis

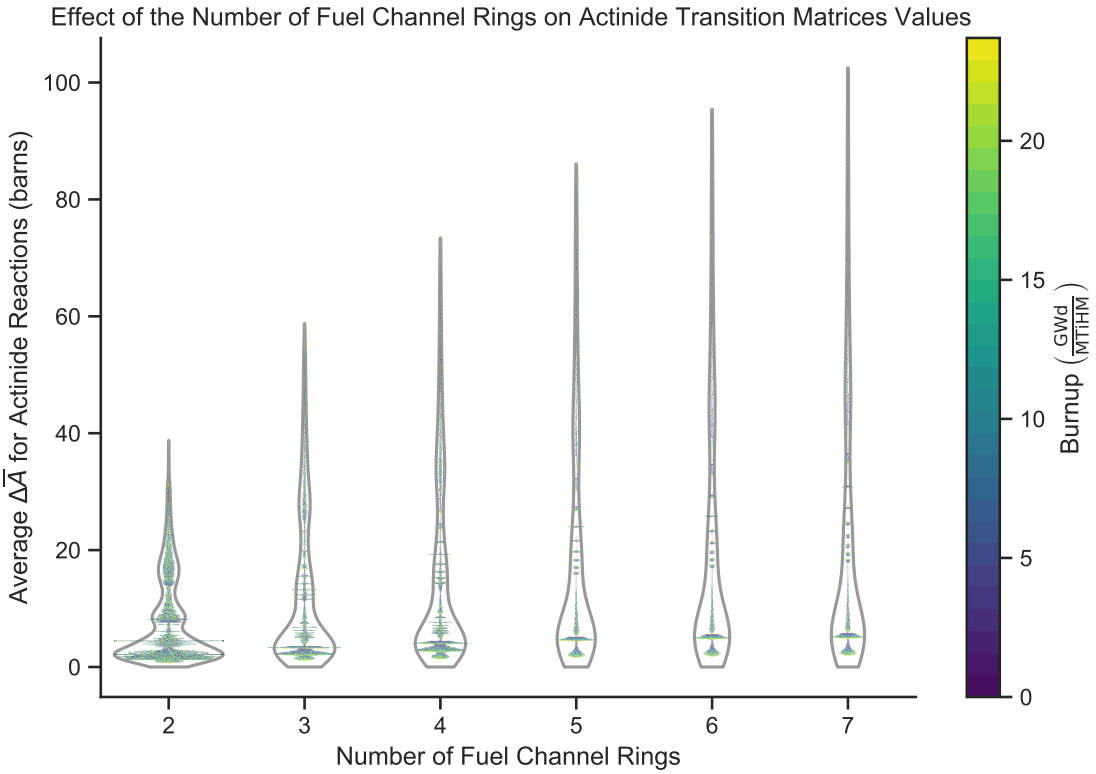

(a) The average difference in transition matrix values compared to libraries with 1 fuel channel ring.

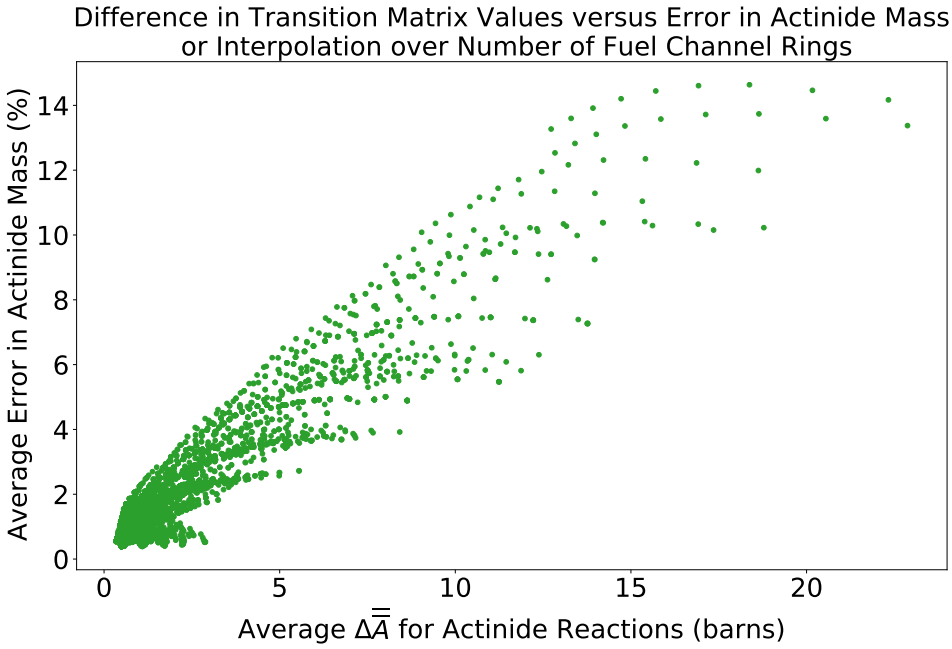

(b) The difference in transition matrix values versus error in actinide mass for interpolating over the number of fuel channel rings for all single spacing possibilities.

Figure 3.4: Fuel Channel Rings Transition Matrix Analysis

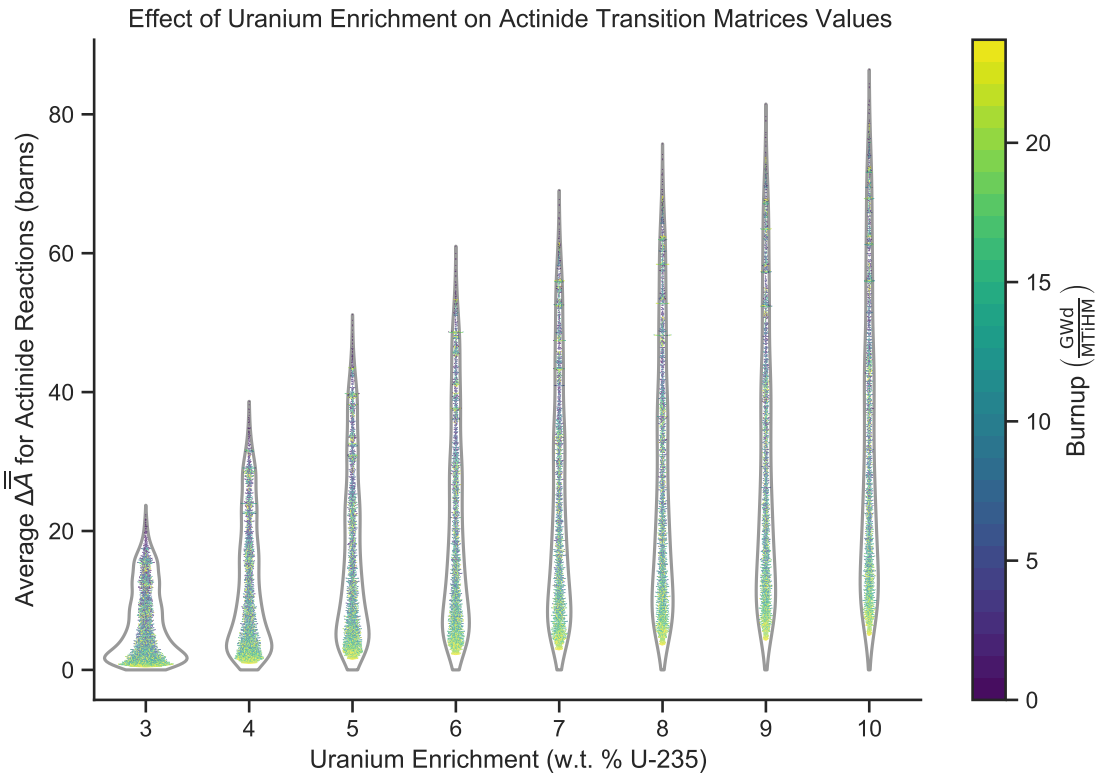

(a) The average difference in transition matrix values compared 2% uranium enrichment libraries.

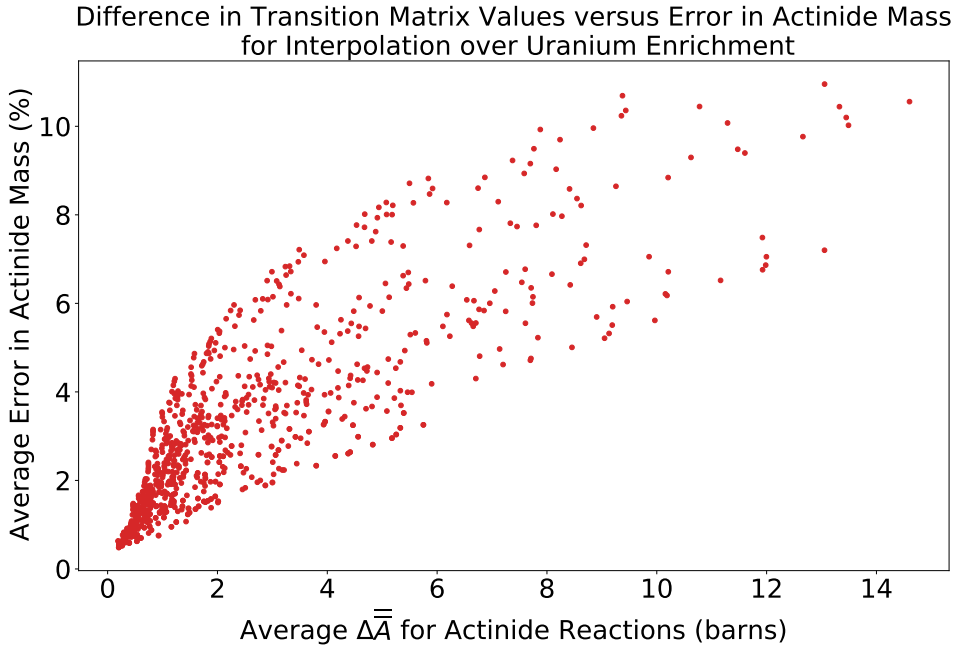

(b) The difference in transition matrix values versus error in actinide mass for interpolating over uranium enrichment for all single spacing possibilities.

Figure 3.5: Uranium Enrichment Transition Matrix Analysis

3.3.2 Single Parameter Spacing

The ideal spacing for each individual parameter was found using both the transition matrix method and from the ORIGEN calculated error in mass. These spacings are shown in Tables 3.4 - 3.8. All possible number of parameter points were tested for each parameter. As before, the uranium enrichment parameter was calculated with a limited number of libraries for inclusion of the actinide mass error.

The ideal spacings calculated by the transition matrix method and from ORIGEN were the same in all but one case. This occurs in the lattice radius parameter with four libraries where the transition matrix method calculates 10 (cm) and 15 (cm) for the inner libraries and the ORIGEN method calculates 10 (cm) and 20 (cm) for the inner libraries. This is not a significant issue however as the difference in error between the two spacings is less than 0.08%. The overall good agreement between the two methods shows the validity of the transition matrix method in this test case.

Table 3.4: Ideal parameter spacing for salt fraction.

Parameter Points	**Parameter Combination (cm)**	**Difference in Transition Matrix Values (barns)**	**Error in Actinide Mass (%)**
2	0.1, 0.5	15.74	12.45
3	0.1, 0.3, 0.5	5.06	3.87
4	0.1, 0.2, 0.3, 0.5	2.64	2.99

Table 3.5: Ideal parameter spacing for lattice radius based on transition matrix values.

Parameter Points	**Parameter Combination (cm)**	**Difference in Transition Matrix Values (barns)**	**Error in Actinide Mass (%)**
2	5, 25	11.35	8.92
3	5, 15, 25	4.58	3.30
4	5, 10, 15, 25	3.91	2.82

Table 3.6: Ideal parameter spacing for number of fuel channel rings.

Parameter Points	**Parameter Combination (-)**	**Difference in Transition Matrix Values (barns)**	**Error in Actinide Mass (%)**
2	1, 7	5.61	4.74
3	1, 3, 7	2.11	1.87
4	1, 2, 4, 7	1.25	1.20
5	1, 2, 3, 5, 7	0.84	0.94
6	1, 2, 3, 4, 5, 7	0.62	0.75

Table 3.7: Ideal parameter spacing for uranium enrichment, limited to half of libraries.

Parameter Points	**Parameter Combination (w.t. % U-235)**	**Difference in Transition Matrix Values (barns)**	**Error in Actinide Mass (%)**
2	0.02, 0.1	4.29	5.69
3	0.02, 0.06, 0.1	1.37	1.53
4	0.02, 0.04, 0.06, 0.1	0.72	0.95

Table 3.8: Ideal parameter spacing for uranium enrichment for all libraries.

Parameter Points	**Parameter Combination (w.t. % U-235)**	**Difference in Transition Matrix Values (barns)**
2	0.02, 0.1	3.88
3	0.02, 0.05, 0.1	1.07
4	0.02, 0.04, 0.07, 0.1	0.53
5	0.02, 0.04, 0.06, 0.08, 0.1	0.35
6	0.02, 0.03, 0.04, 0.06, 0.08, 0.1	0.25
7	0.02, 0.03, 0.04, 0.05, 0.06, 0.08, 0.1	0.18
8	0.02, 0.03, 0.04, 0.05, 0.06, 0.07, 0.08, 0.1	0.14

Figure 3.6 shows the average correlation between the difference in transition matrix values and the error in actinide mass between interpolated and generated reactor libraries for a given parameter combination. The correlation between the two values is much stronger when looking at the parameter combination as a whole rather than individual libraries and follows a linear fashion.

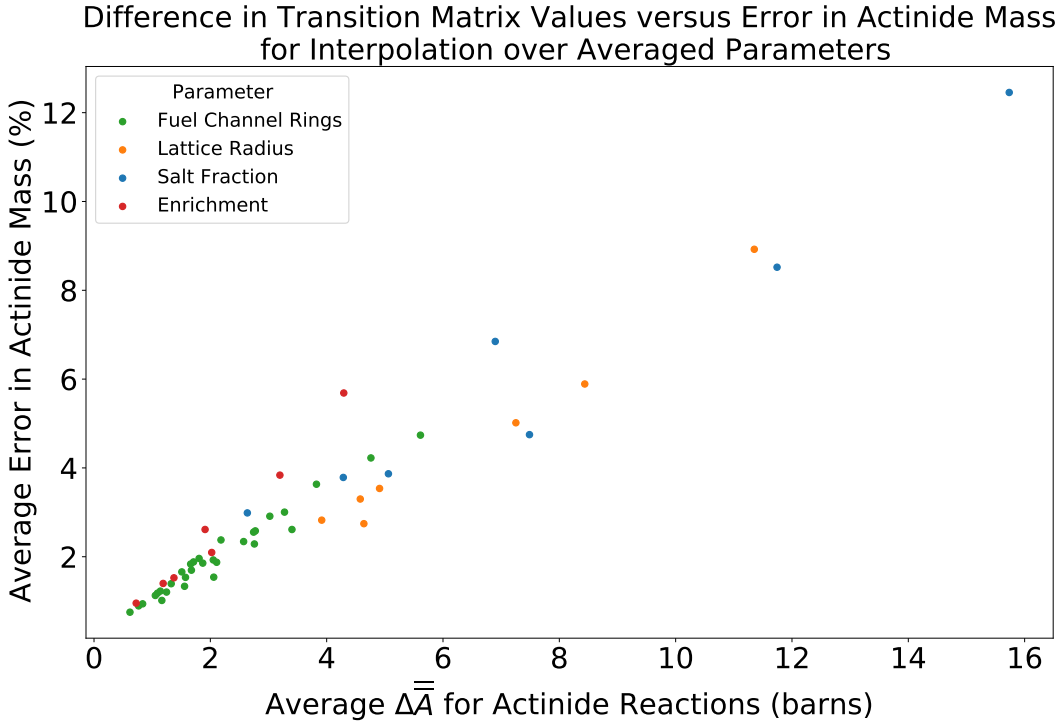

Figure 3.6: The average difference in transition matrix values versus the average error in actinide mass from interpolation for all single parameter spacing combination.

Chapter 4

Fission Product Removal in ORIGEN Reactor Libraries

4.1 Introduction

The ability to separate fission products from the fuel salt is a key aspect to many molten salt reactor designs. The removal of fission products allows for many benefits, including: improved neutronics performance (i.e., by reducing parasitic capture), the reduction of the reactor's core accident source term, and the removal of corrosion-inducing elements. The removal of fission products will lead to a variety of effects relevant for material control & accounting. The most important of these effects include: a change in the amount of fissile material within the salt, a change in the composition the salt, and a change in the length of time the reactor is critical.

This chapter includes three main parts. The first part is a description of a model for studying the effects of fission product removal in MSRs. The second part is a detailed analysis of this model. The final part details the development of a methodology for capturing the effects of fission product removal while using ORIGEN reactor libraries.

4.2 Fission Product Removal Model

4.2.1 Model Description

The base model for analysis is a single-fluid, fluoride-uranium hexagonal lattice pin as shown in Figure 4.1. Additional model attributes are shown in Table 4.1. The model was run using the TRITON-NEWT sequence within SCALE 6.3b5.

The model was run as a pin-cell rather than a quarter-core primarily for debugging reasons. The material addition and removal feature in TRITON required extensive work to use because of its developmental nature. The code to produce a pin-cell model was smaller, faster to run, and more comparable to existing example models, making debugging easier. Unlike the previous analysis the size of the reactor core was not a changing variable in this model, therefore a pin-cell is assumed a reasonable representation of the reactor system.

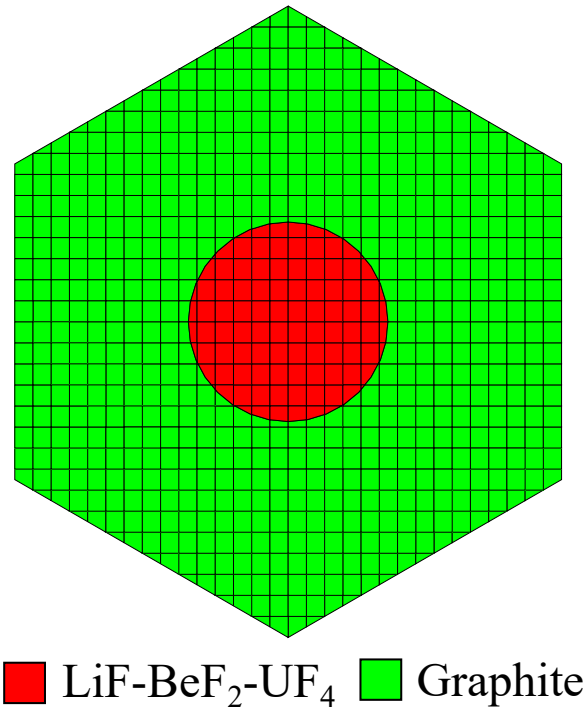

Figure 4.1: SCALE model geometry. The grid pattern depicts the meshing of the model.

Table 4.1: Model Attributes

Attribute	**Value**
Power	20 MW
Salt Temperature	923 K
Salt Density	3.353 g/cm^3
Uranium Enrichment	5% U-235
Li-7 Enrichment	99.995 %
Graphite Temperature	950 K
Graphite Boron Concentration	1.503 ppm
Fuel Channel Radius	2.7282
Graphite Pitch	7.5
Cycle Length	3000 Days
Fuel Loading	1 MTHM

4.2.2 Fission Product Removal

Two different fission product removal systems were included in the model, a gas sparging system and a salt processing system. The isotopes removed were based on previous analysis of the single-fluid double-zone thorium molten salt reactor [1]; elements that were not available in the TRITON sequence were excluded from analysis. The full list of elements removed is shown in Table 4.2. Additionally, the table gives a brief description of each group of elements and a key.

The gas sparging and salt processing systems were analyzed over three different cases. In Case 1 only the gas sparging system was modeled, in Case 2 only the salt processing system was modeled, in Case 3 both systems were modeled. In each case the grouped fission product removal rate constant was varied from $3.333 \cdot 10^{-1}$ to $3.333 \cdot 10^{-10}$ (1/s) with ten equally spaced values on a logarithmic scale. Additionally, a base run with no fission product

removal was included in each case. For Case 3 the cross-product terms were included giving a total of 121 different variations of removal rates.

4.2.3 Model Validity

Extensive testing was done to ensure that the material removal feature in TRITON worked as expected. Three types of tests were run on models similar to the one used for analysis.

In the first test the underlying equations for material removal were tested. The test was conducted by comparing the amount of material removed by TRITON versus the analytical solution of the equations governing material removal. To easily solve these equations the reactor power was set to zero and a non-decaying material was removed. With these constraints the differential equation describing material removal is defined by Equation 4.1, where N_i is the select nuclide, λ is the removal constant, and t is time. The solution to this equation is shown in Equation 4.2.

Table 4.2: Description of fission product groups and their isotopes.

Processing System	**Description**	**Elements**	**Key**
Gas Sparging	Gaseous and Non-Dissolved Metal Fission Products	H, He, N, O, Ar, Kr, Nb, Mo, Tc, Ru, Rh, Pd, Ag, Sb, Te, Xe, Lu, Hf, Ta, W, Re, Ir, Au	R1
Salt Processing	Lanthanides and other Soluble Fission Products	Ga, Ge, As, Se, Br, Rb, Sr, Y, Zr, Cd, In, Sn, I, Cs, Ba, La, Ce, Pr, Nd, Pm, Sm, Eu, Gd, Tb, Dy, Ho, Er	R2

$$\frac{dN_i}{dt} = N_i \cdot -\lambda \tag{4.1}$$

$$N(t) = N_0 \cdot e^{-\lambda \cdot t} \tag{4.2}$$

In the second test the physical convergence of the material removal feature was tested. This was done by continuously decreasing the removal rate of fission products in a model until the results converged upon that of a model with no removal. Physically as the removal of fission products is decreased the behavior of the system should converge to the same as to when no fission products were being removed.

The final test done was analyzing the effect of depletion time steps on fission product removal. This test was done by comparing three models with increasingly larger time steps. The mass of fission products and critically of the system was then compared across the models.

Although simple these tests revealed issues with using the material addition and removal feature that possibly would not have been noticed otherwise. One major issue found through the second test was that the setting for adding trace nuclides to the fuel composition needed to be changed from its default value to its highest possible value to achieve correct results with the model (TRITON parameter addnux=4).

4.3 Model Analysis

The obvious direct effect on a system from removing fission products is that the quantity of fission products in the system is decreased. A useful corollary to the quantity of fission products in the system is the effective one-group removal cross-section of fission products. By grouping the fission products into a single term their overall effect on the system can easily be understood.

Figure 4.2a shows the effective one-group removal cross-section of the gaseous and non-dissolved metal fission products in the core for Case 1. At high removal rates the fission products are effectively gone throughout the entire reactor cycle. When the removal rate is

lowered the effective cross-section of the fission products begins to rise. For high removal rates the effective cross-section of fission products is nearly constant over time, however at lower removal rates the effective cross-section rises significantly with time. Figure 4.2b shows the effective removal cross-section of the lanthanides and soluble fission products in the core for Case-2. The overall trends of the effective cross-sections are similar to that of in Case-1, albeit with differing values.

Indirectly, the removal of fission products will have a number of effects on a system. One such effect is the softening of the neutron spectrum in the core as isotopes with large thermal capture cross-sections are removed. To determine the magnitude of this change the neutron spectra of Case 1 and Case 2 were compared to the base case with no fission product removal. Figure 4.3 shows the time-averaged energy-dependent neutron flux for the base case, which is referred to as the 'R0' flux.

Figures 4.4a and 4.4b shows the fluxes of Cases 1 and 2 relative to the R0 flux. The removal of fission products causes a thermalization effect in both cases. As the removal rate is increased the magnitude of thermalization is also increased in both cases. The shape of thermalization in the spectrum is similar between the two cases. Additionally, the overall magnitude of thermalization can be seen to be correlated to the effective cross-section of the fission products.

Another effect the removal of fission products has on the system is the changing the actinide generation and depletion rate. This effect is driven by the change in neutron spectrum and causes significant differences in the mass of actinides. Figures 4.5a and 4.5b shows the differences in major actinide masses for Case 1 and 2 relative to the base case with no fission product removal.

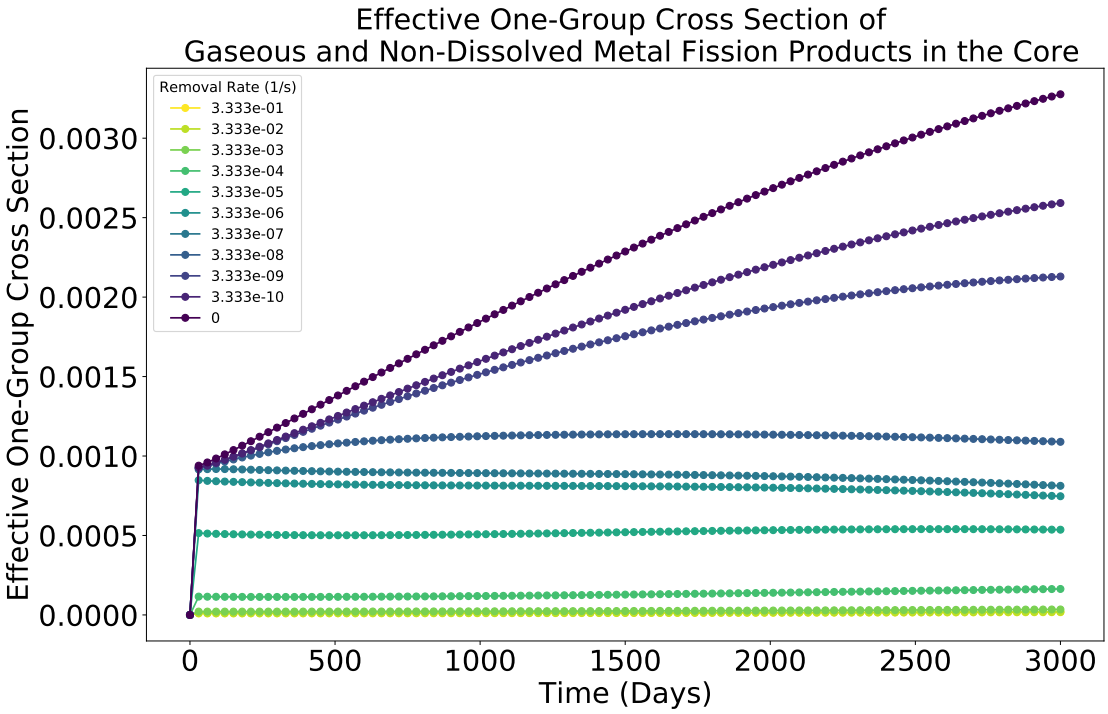

(a) Case 1 - Fission products removed with gas sparging system.

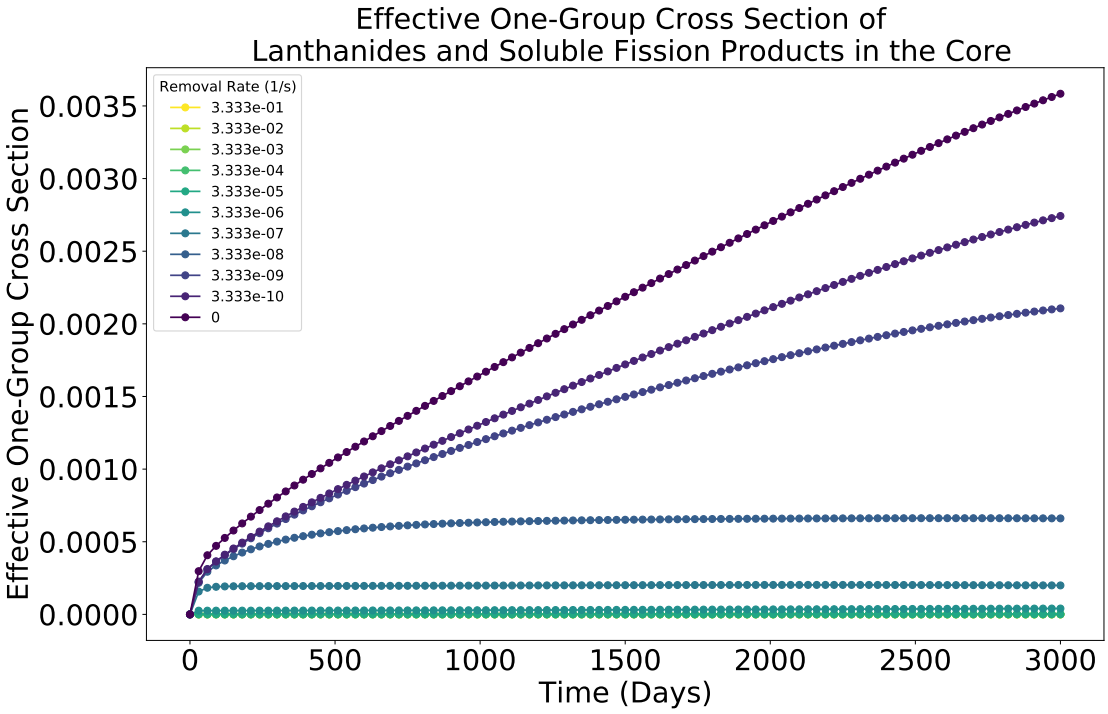

(b) Case 2 - Fission products removed with salt processing system.

Figure 4.2: Effective one group cross-sections of fission products in the core for varying removal rates.

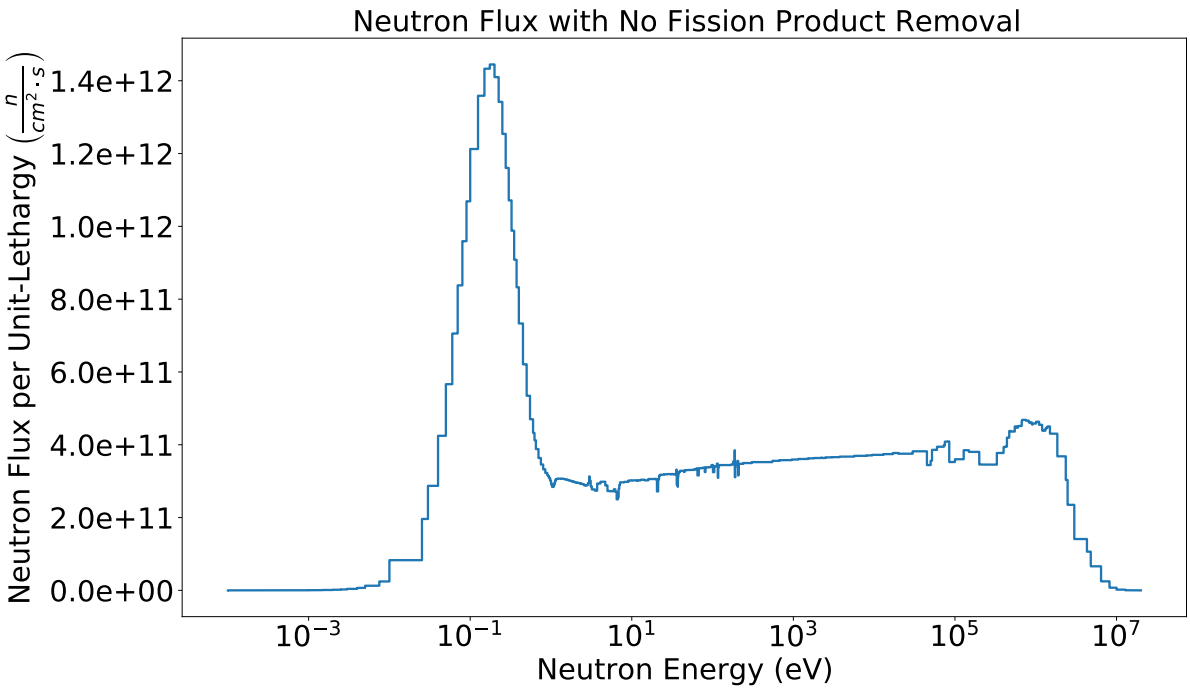

Figure 4.3: Cycle averaged neutron flux spectrum of base model with no fission product processing.

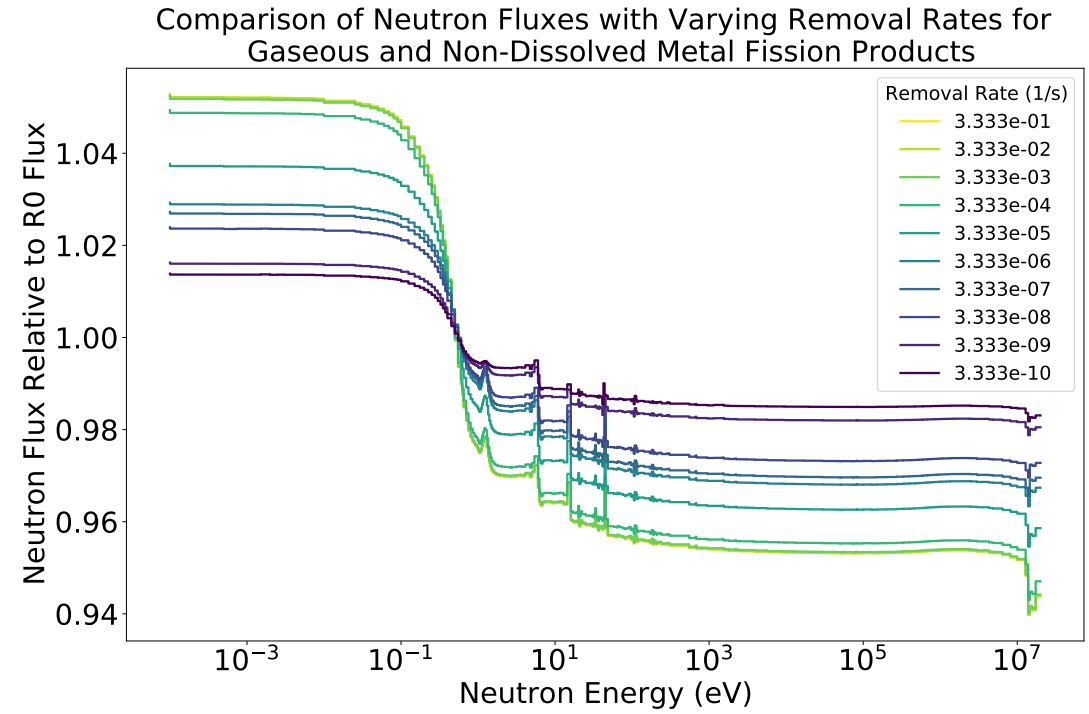

(a) Case 1 - Fission products removed with gas sparging system.

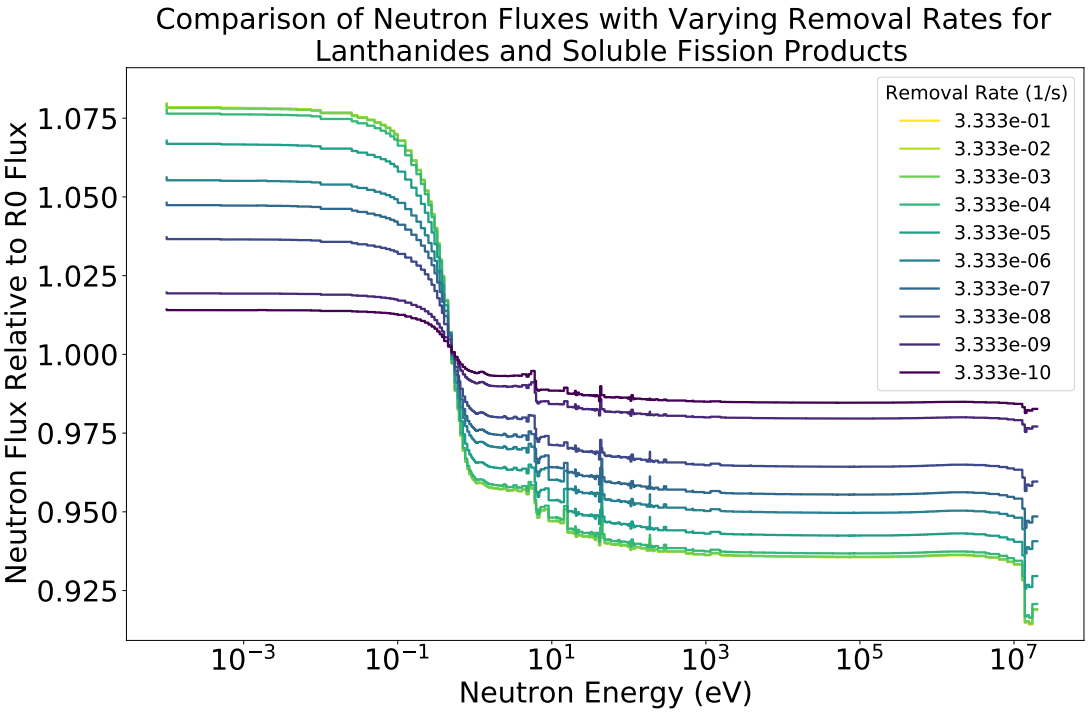

(b) Case 2 - Fission products removed with salt processing system.

Figure 4.4: Cycle averaged energy-dependent neutron flux of Cases 1 & 2 relative to the base flux.

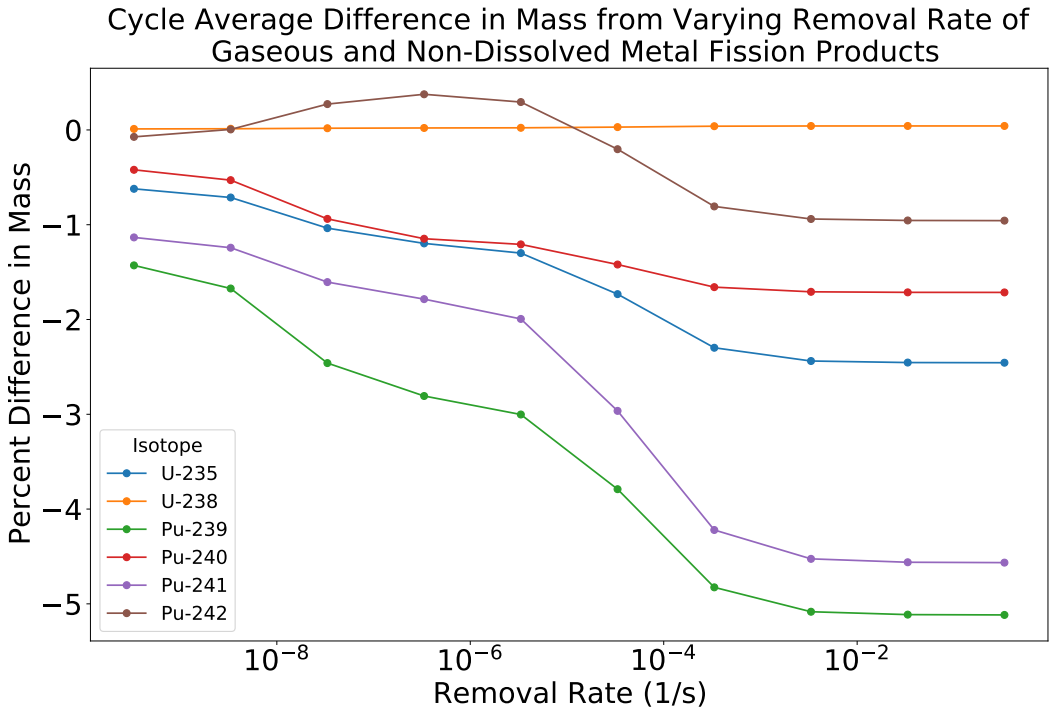

(a) Case 1 - Fission products removed with gas sparging system.

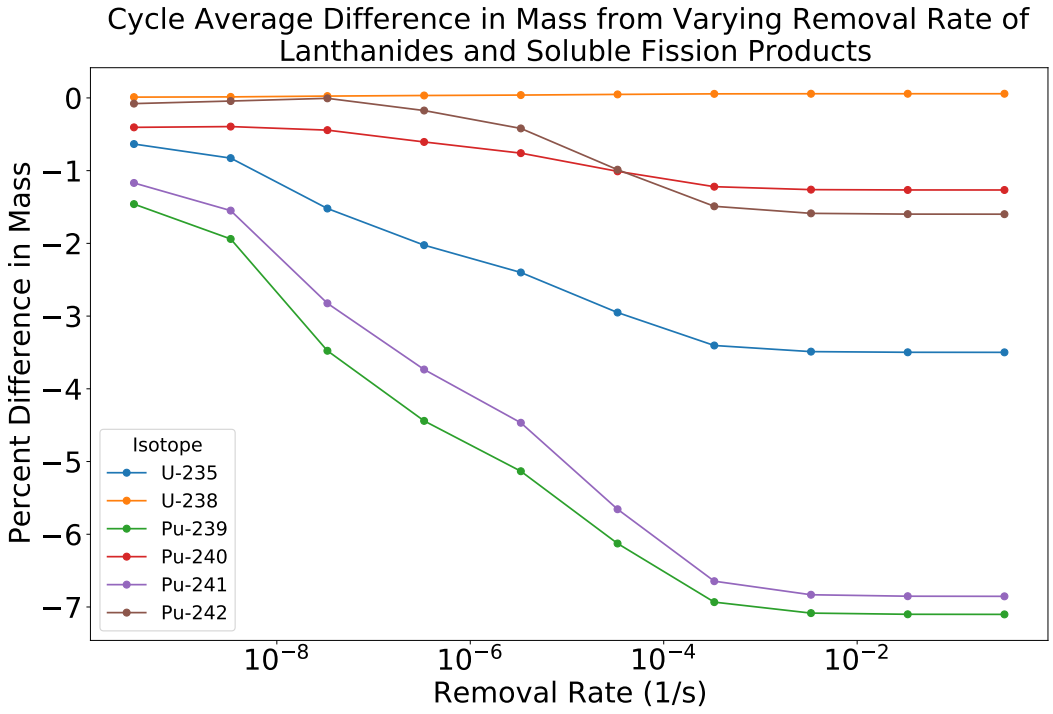

(b) Case 2 - Fission products removed with salt processing system.

Figure 4.5: Cycle-averaged mass difference in actinides for Cases 1 & 2 relative to the base case.

In both cases the mass of U-235 in the system decreases as the removal rate is increased. In other words, more U-235 is burned as more fission products are removed. Additionally, the net generation of Pu-239, Pu-240, and Pu-241 decreases as the removal rate is increased in both cases. The combination of both of these effects means that the removal of fission products leads to an overall lower mass of fissile material in the system when power is held constant across cases. This can be partially understood from comparing the fluxes between the removal and non-removal cases. The thermal flux is higher in the removal case, while the total flux is lower (i.e., there is less total flux to transmute U-238 into plutonium and there is more thermal flux to fission U-235).

4.4 ORIGEN Reactor Library Methodology

A methodology was created and tested for including fission product removal in the ORIGEN reactor libraries. The two main objects of methodology were to (1) be able to accurately capture the changes in major actinides with ORIGEN and (2) minimize the number of libraries needed. The methodology was created to be able to solve for any of the values of removal rates within Case 1, 2, and 3. This was done in two parts, the first part allows for the interpolation over a single removal group, while the second allows for the interpolation of both removal groups simultaneously.

4.4.1 Single Removal Group Interpolation

The logical first approach to implement interpolation would be to interpolate over the variable being change, in this case removal rate. However, there is an immediate apparent problem with this approach: the values of removal rates span many orders of magnitude. Interpolating over this range would heavily skew the solution towards lower removal rates. Furthermore, a logarithmic function cannot be easily applied to solve the problem. This is because a composite function is needed as a removal rate of zero is included in our set of rates. Determining this composite function would require fitting the removal rate to some other variable.

Nevertheless, interpolation over removal rate was carried out to determine the plausibility of the approach. Figure 4.6a and 4.6b show the error in actinide masses when interpolating over removal rate. For the interpolation two libraries were used, one at a removal rate of 0.3333 (1/s) and one at 0 (1/s). As predicted the errors are higher at lower removal rates. Overall, the errors are fairly significant, for some isotopes the error from interpolation is greater than the induced mass difference from removing fission products.

Due to the high errors a different approach is necessary. One such way would be to interpolate over the physical effect of removing fission products, rather than the removal rate itself. The previous model analysis laid out the direct physical effect of removing fission products as being a change in the mass of the fission products, or in a different form the effective one-group cross-section of these fission products.

Therefore, a second approach was attempted by interpolating over the time-averaged effective one-group removal cross-sections of the elements being removed. To carry this out a fitted function was created for each removal group that correlated the removal rate to the effective one-group cross-section. The fitted functions are shown in Equation 4.4.1 and 4.4.1 for groups R1 and R2 respectively.

$$f_1(x) = \begin{cases} 0.002201 & x = 0 \\ -(0.00076 + 0.00012 \cdot ln(x)) & 0 < x < 0.003333 \\ 0 & 0.003333 \leq x \end{cases}$$

$$f_2(x) = \begin{cases} 0.00212 & x = 0 \\ -(0.00323 + 0.00023 \cdot ln(x)) & 0 < x < 3.333 \cdot 10^{-6} \\ 0 & 3.333 \cdot 10^{-6} \leq x \end{cases}$$

Figure 4.7a and 4.7b plot these functions along with the actual one-group cross-section for each group. Additionally, the graphs show the coefficient of determination for the fit. The function appears to be a good fit both from visual analysis and the r^2 measure. The fit for group R1 has the largest variation in removal rates that range from 10^{-8} 10^{-4} (1/s), while the fit for group R2 has the largest in removal rates that are below 10^{-7} (1/s).

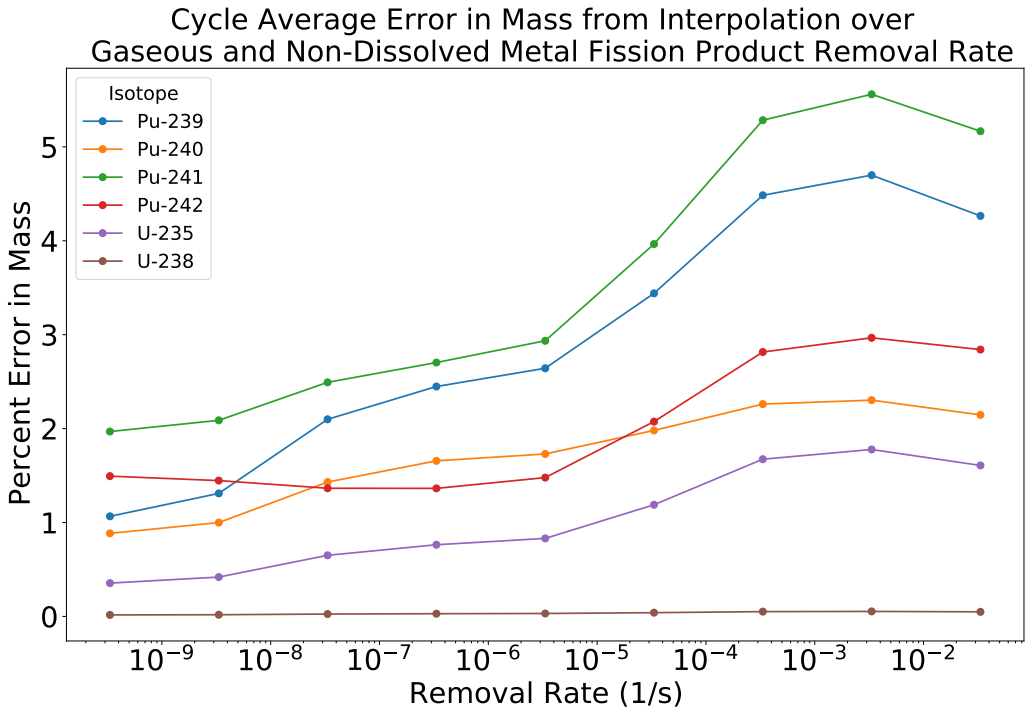

(a) Case 1 - Fission products removed with gas sparging system.

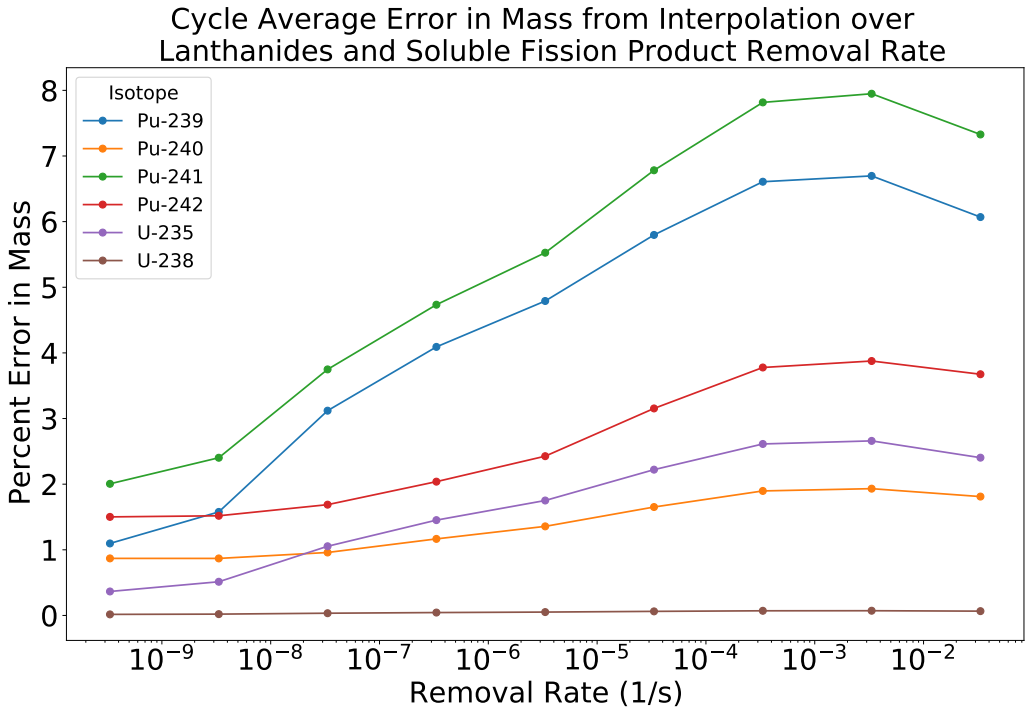

(b) Case 2 - Fission products removed with salt processing system.

Figure 4.6: Cycle average error in mass from interpolation over removal rate.

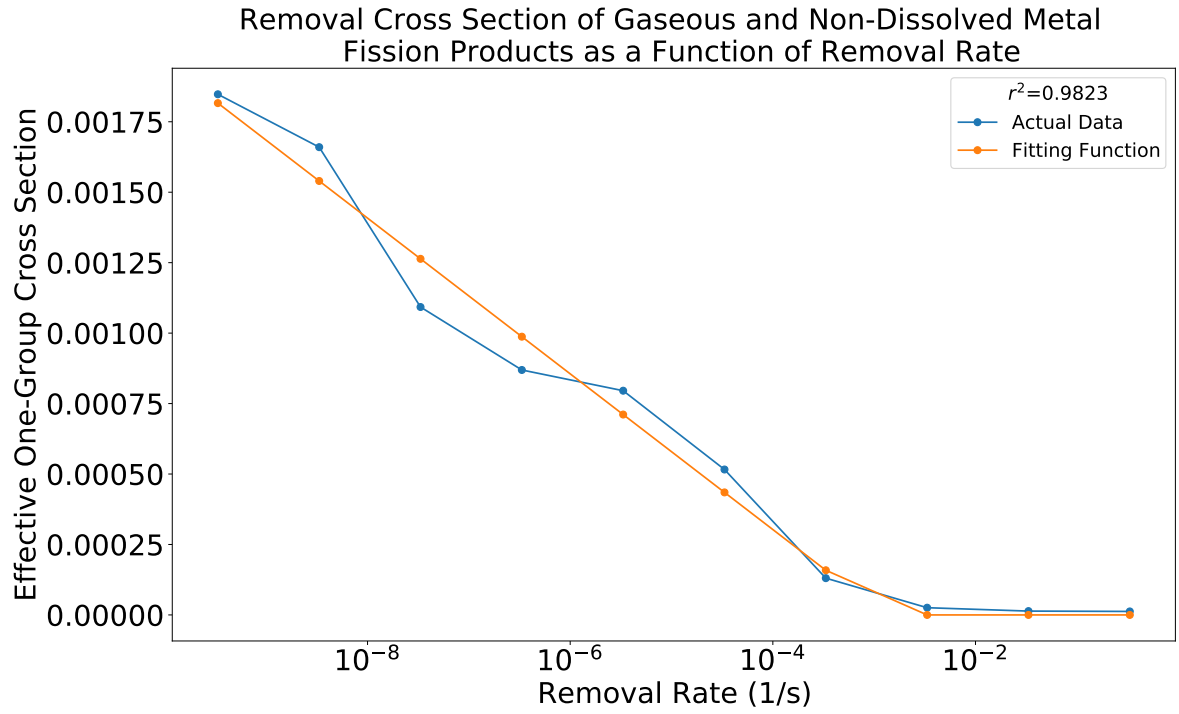

(a) Case 1 - Fission products removed with gas sparging system.

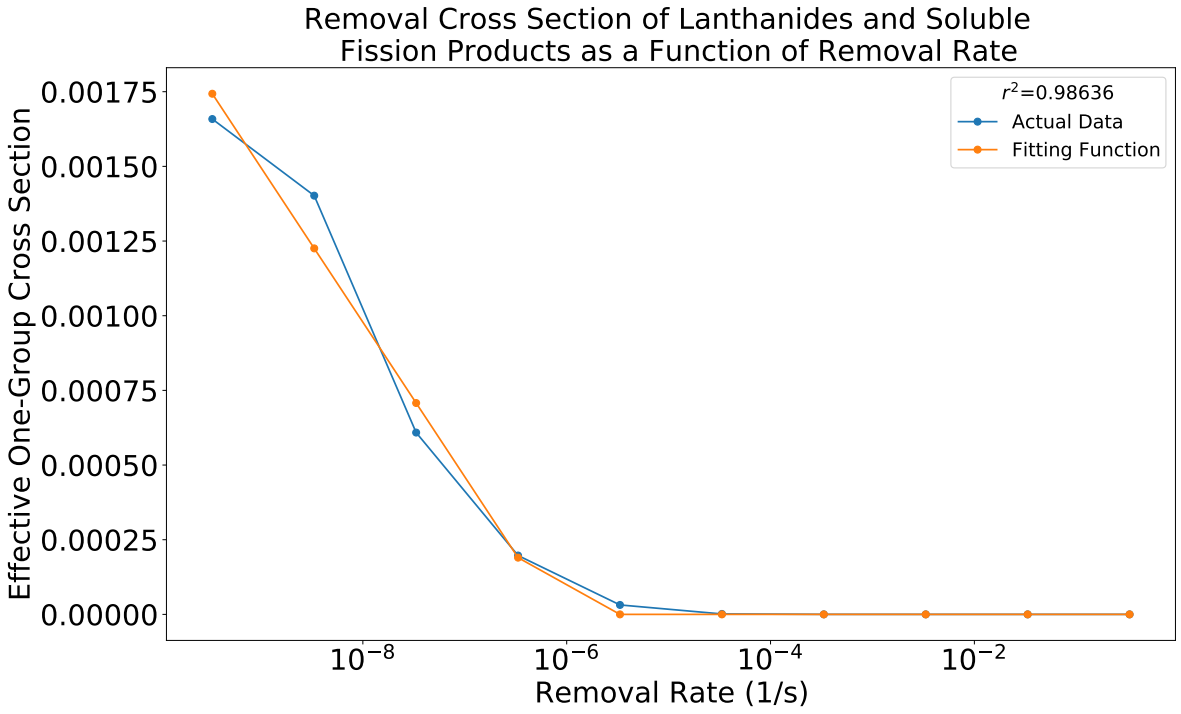

(b) Case 2 - Fission products removed with salt processing system.

Figure 4.7: Fitting functions for effective one-group removal cross-sections along with cross-section data.

Interpolation was carried out using the new fitted functions, again with two libraries at the highest and lowest removal rate. Figures 4.8a and 4.8b show the error in actinide masses from this interpolation. The error is only shown at the interpolated points at not at the end points (i.e., removal rates of 0 and 0.3333 (1/s). The error in interpolation from the second approach is significantly less than the error from interpolation over removal rate. The magnitude of the error does not directly follow the difference between the fitting function for the removal cross-section and the actual removal cross-section. At relatively low errors other effects are likely driving the magnitude of the error such as the time-dependence of the cross-sections.

4.4.2 Dual Removal Group Interpolation

Interpolating over libraries with both removal groups is a more challenging problem because of the large number of combinations of removal rates. Interpolating over removal rates was not attempted at all, instead interpolation over effective removal cross-sections was used as a starting point.

In the original model analysis two important observations were made. First, the difference in actinide depletion and generation is caused by a thermalization of the neutron spectrum. Secondly, the thermalization from the two fission product groups is similar in shape, and the magnitude of the shape is driven by the one-group effective removal cross-sections. Therefore, it should be possible to achieve the correct actinide masses in the system by interpolating over all fission products as a single combined group.

This method was tested by interpolating over the two libraries with the minimum and maximum combined removal rates. To do this, the already found individual group fitting functions were added together to form a function that calculates the combined effective one-group removal cross-section of both groups. The two libraries were then interpolated to every removal rate combination. The interpolated libraries were run in ORIGEN and compared to the results of TRITON calculations.

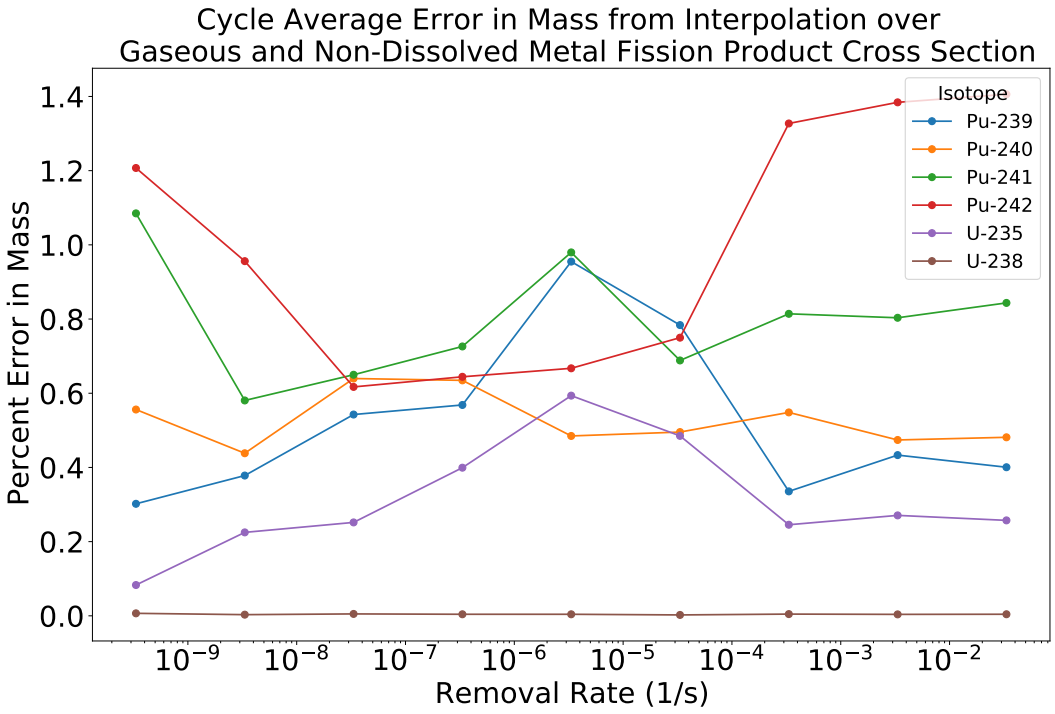

(a) Case 1 - Fission products removed with gas sparging system.

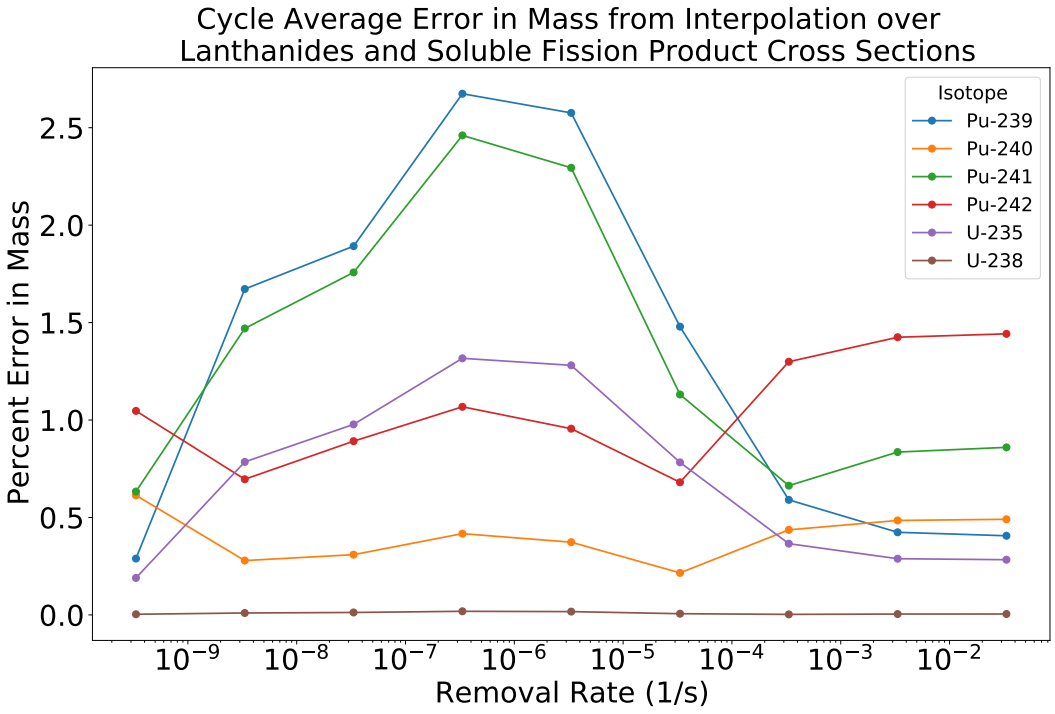

(b) Case 2 - Fission products removed with salt processing system.

Figure 4.8: Cycle average error in mass from interpolation over effective one-group removal cross-section of fission products being removed.

Figures 4.9 through 4.14 shows the mass percent error between the interpolated libraries and TRITON generated libraries for the major actinides. The white "L"s mark the two libraries used for interpolation. The errors for U-235, U-238, Pu-239 and Pu-240 are all fairly low and comparable to the single removal group method. In this test case the errors for Pu-241 and Pu-242 are significant compared to the induced actinide differences from fission product removal. The errors are high at low R1 rates and high R2 rates which corresponds to the largest quadratic distance between the interpolation points. The error at a high R1 rate and low R2 rate are not as high (i.e., the error is not symmetrical).

Overall, this approach for capturing the effect of fission product removal was deemed reasonable as the error in actinide mass was low in most combinations of removal rates. If necessary, the error could be further reduced by either adding additional libraries or limiting the range of removal rates within the set of libraries.

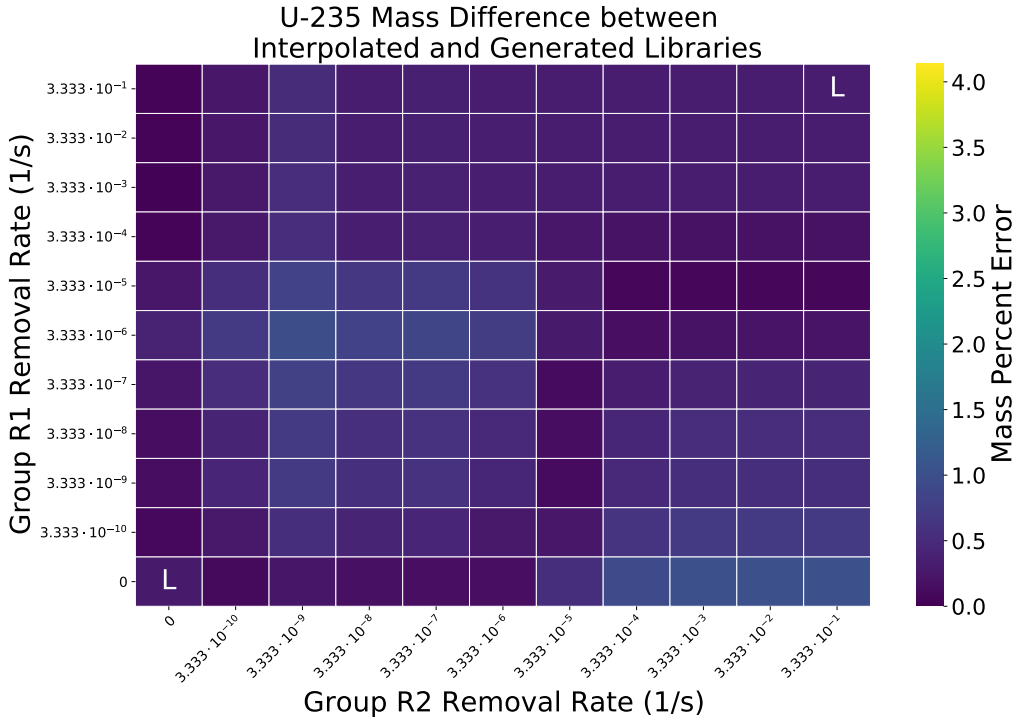

Figure 4.9: Cycle averaged error in U-235 mass from interpolation over combined cross-sections.

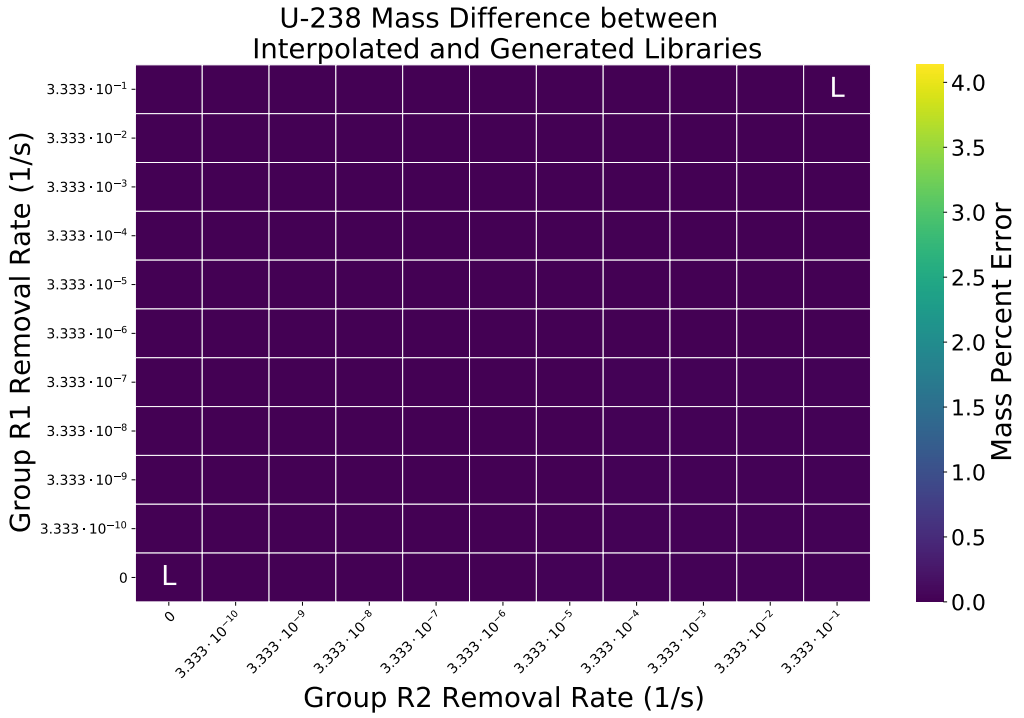

Figure 4.10: Cycle averaged error in U-238 mass from interpolation over combined cross-sections.

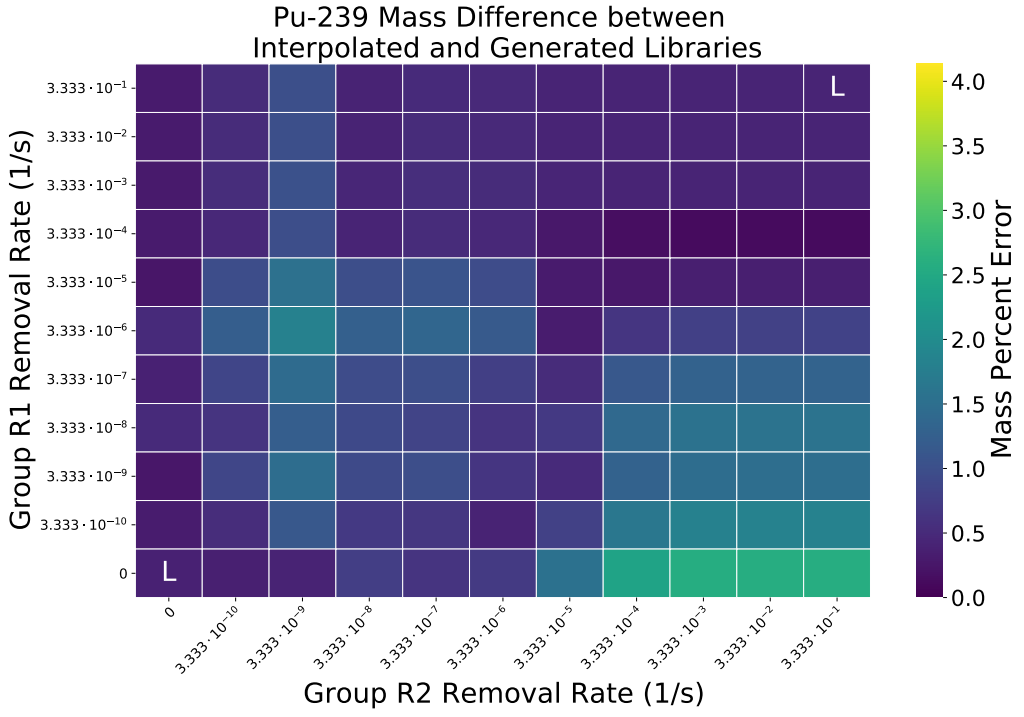

Figure 4.11: Cycle averaged error in Pu-239 mass from interpolation over combined cross-sections.

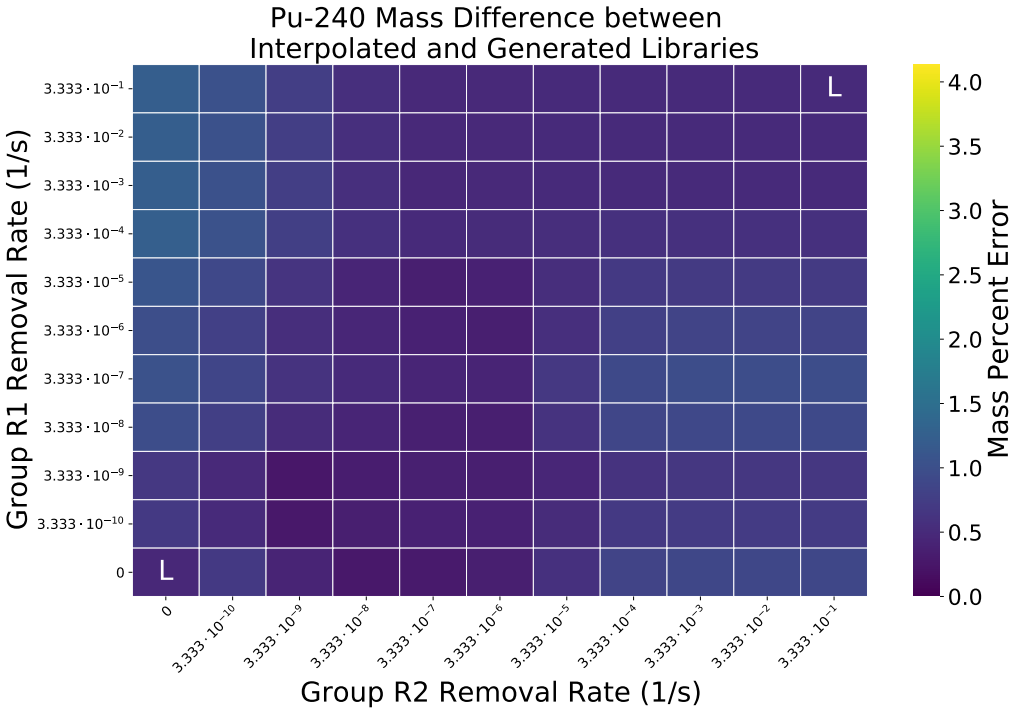

Figure 4.12: Cycle averaged error in Pu-240 mass from interpolation over combined cross-sections.

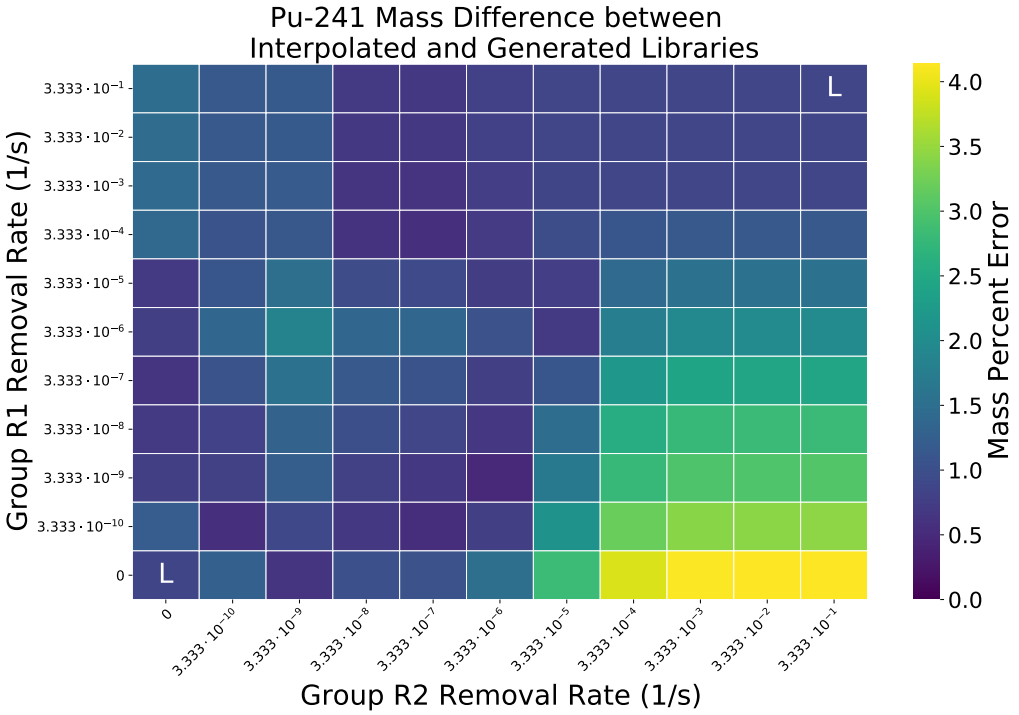

Figure 4.13: Cycle averaged error in Pu-241 mass from interpolation over combined cross-sections.

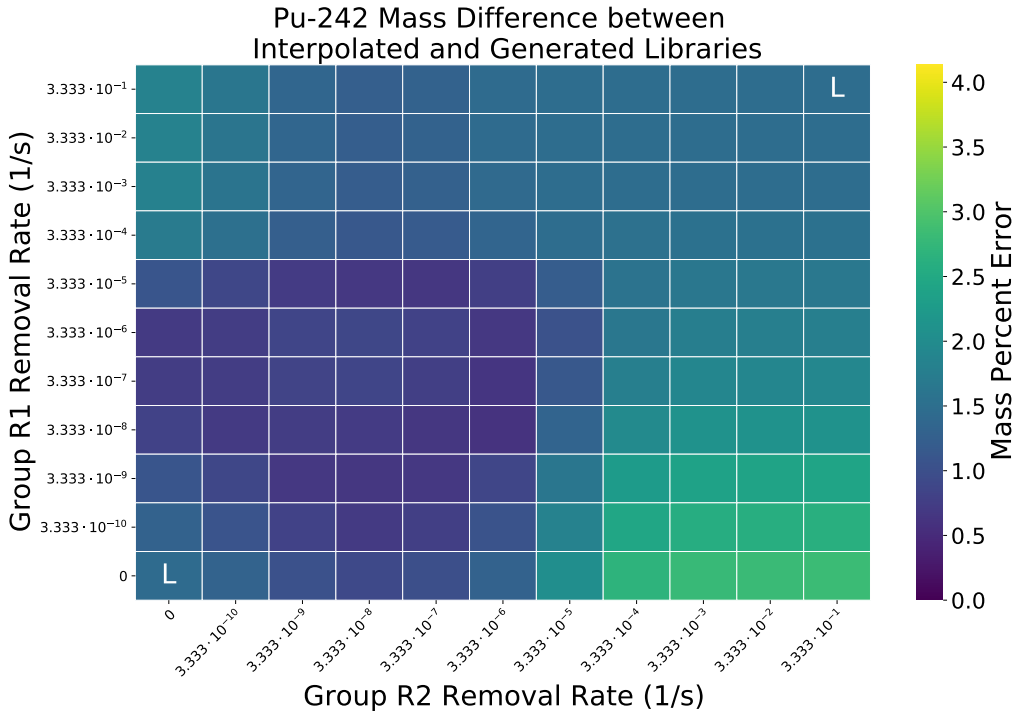

Figure 4.14: Cycle averaged error in Pu-242 mass from interpolation over combined cross-sections.

Chapter 5

Online Refueling in ORIGEN Reactor Libraries

5.1 Introduction

The ability to refuel while operating is an integral component of many proposed MSR designs. Online refueling allows for many benefits including: continuous operation, limiting the required excess reactivity within the core, and a larger number of fuel cycle choices among others. Correctly modeling online refueling is critical in neutronic, fuel cycle, and MC&A analyses as refueling directly changes the fissile mass and spectral characteristics of the reactor.

The structure of this chapter and its analysis follows closely to that of Chapter 4. The first part of the chapter is a description of the model used to study online refueling. The second part is a brief analysis of the model. The third part details efforts to incorporate online refueling into ORIGEN reactor libraries with interpolation

5.2 Online Refueling Model

5.2.1 Model Description

The base model for analysis is similar to the model for the fission product removal. The model is a single-fluid, uranium tetrafluoride hexagonal lattice pin. The model geometry is the same as the fission product removal model. The initial fuel enrichment and the refueling feed rate are varied in the model. The values for these parameters are shown in 5.1, the reactor is refueled with 5% enriched uranium. The remaining attributes for the model are shown in Table 5.2.

5.3 Model Analysis

The model was analyzed to determine two effects relevant to interpolation with reactor libraries. The first was to determine the effect that varying the feed rate of refueling has on the reactor system. The second was to determine how the initial condition of the reactor effects the changes caused by varying the feed rate.

The addition of uranium into the core of a reactor is going to have a range of effects on neutronics and fuel depletion. The most direct effect on the system will be the amount of uranium within the core. Figures 5.1a and 5.1b show the mass of U-235 relative to its initial value in the system over time. As expected the feed rate for refueling has a large effect on the mass of uranium in the system.

Table 5.1: Model Parameters and Values

Parameter	Values
Initial Fuel Enrichment (w.t. % U-235)	1, 2, 3, 4 , 5
Refueling Feed Rate (kg/day)	0, 0.1, 0.3, 0.5

Table 5.2: Model Attributes

Attribute	**Value**
Power	20 MW
Salt Temperature	900 K
Salt Density	3.353 g/cm^3
Li-7 Enrichment	99.995 %
Graphite Temperature	900 K
Graphite Boron Concentration	1.503 ppm
Fuel Channel Radius	2.7282
Graphite Pitch	7.5
Cycle Length	400 Days
Fuel Loading	1 MTHM

Importantly the effect of varying the feed rate is dependent on the initial condition of the reactor. This means that for each parameter combination, e.g. initial fuel enrichment, volume of salt, etc., the effect of varying the feed rate will be different. This can be understood better by noting that the amount of U-235 and U-238 mass added is constant for any given feed rate. If the initial fuel enrichment is increased the relative amount of U-235 added for a given feed rate will decrease. Similarly, if the volume of salt in the reactor is increased the relative amount of U-235 and U-238 added for a given feed rate will decrease. It is important to determine if this initial condition effect changes the underlying neutronics of the system as this may affect the reactor library generation and interpolation process. To determine this the fission rate and capture cross-sections of the model were analyzed.

Figures 5.2a and 5.2b shows the ratio of fission rates between Pu-239 and U-235 for varying feed rates of uranium. In all cases the fission rate ratio grows over time as Pu-239 is built up and burned in the core. As the feed rate of uranium to the core is increased the fission rate ratio is decreased. The difference in fission rates due to a change in initial fuel enrichment is significant. The difference in fission rates due to varying the feed rate is much

higher at a 1% U-235 enrichment than a 5% U-235 enrichment. In the 1% U-235 enrichment Pu-239 fissions start to overtake U-235 fission later in the cycle at low feed rates. In both cases for all feed rates the fission rate ratio is never constant, even in the case when the mass of U-235 in the core is nearly constant over time.

Figures 5.3a and 5.3b show the changes in capture cross-sections for key isotopes with varying feed rates of uranium. The change in capture cross-sections due to varying the feed rate becomes smaller as the initial fuel enrichment is increased. The difference in capture cross-sections due to a change in initial fuel enrichment is larger than the difference due to changing the feed rate, i.e., the initial enrichment is a more strongly dominant effect than the feed rate.

5.4 ORIGEN Reactor Library Methodology

5.4.1 Feed Rate Interpolation

Figure 5.4 shows the cycle average error in mass between an ORIGEN solution and a TRITON solution for varying uranium feed rates. A single ORIGEN library was used, which was generated with no uranium feed. The correct feed rates were included in the ORIGEN calculations. The reference TRITON solutions were all generated with uranium feed. The error between the ORIGEN and TRITON calculation increases as the feed rate is increased. To a first-order the increasing error in the isotopes can be explained by the cross-sections changes that occur when the feed rate is increased (as was seen in the previous section). Depending on the tolerable error, feed rate, and cycle length an ORIGEN library generated with uranium feed might not be necessary.

Figure 5.5 shows the cycle average error in mass between an ORIGEN solution and a TRITON solution for varying uranium feed rates. In this calculation the reactor libraries at a feed rate of 0 and 0.5 (kg/day) are directly generated from TRITON with their respective feed rates. The transition coefficients corresponding to 0.1 and 0.3 (kg/day) were linearly interpolated between the libraries at 0 and 0.5 kg/day. By including a second library and interpolating the error is able to be significantly reduced.

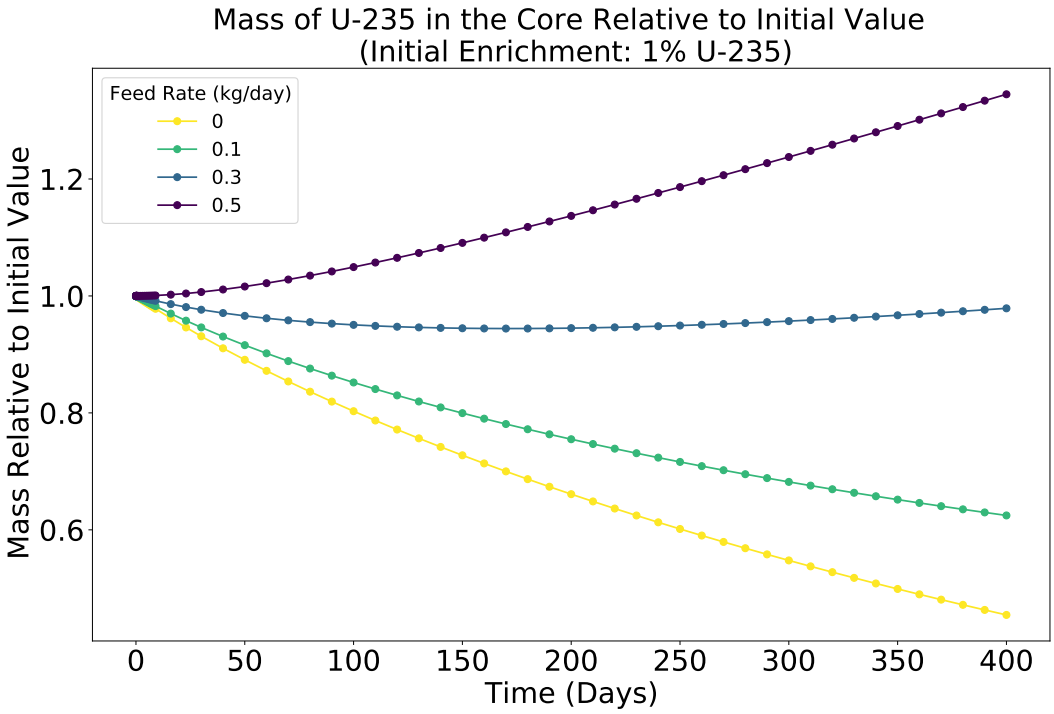

(a) Initial Fuel Salt Enrichment of 1% U-235

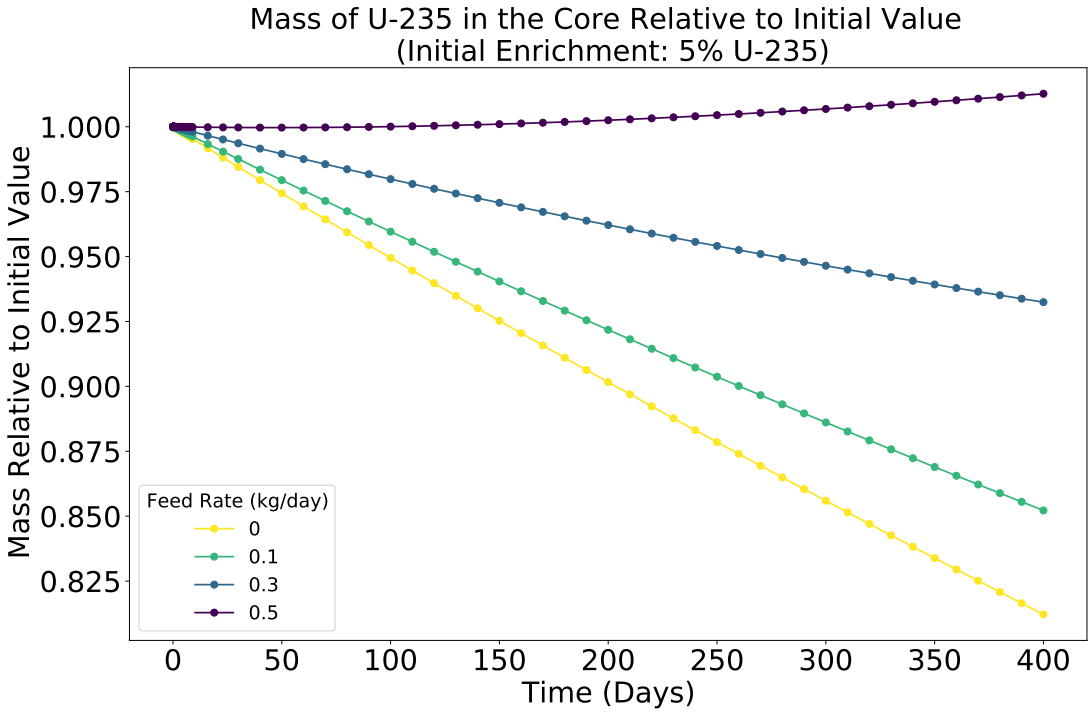

(b) Initial Fuel Salt Enrichment of 5% U-235

Figure 5.1: Mass of U-235 in the core over time relative to the initial amount of U-235 in the core for varying feed rates of uranium.

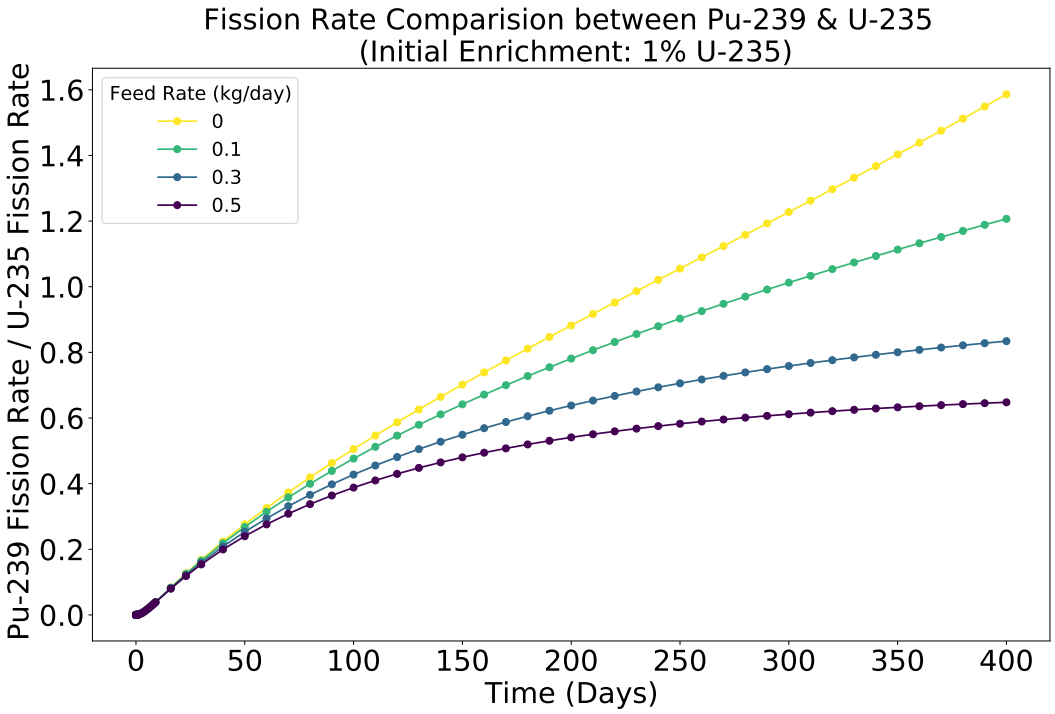

(a) Initial Fuel Salt Enrichment of 1% U-235

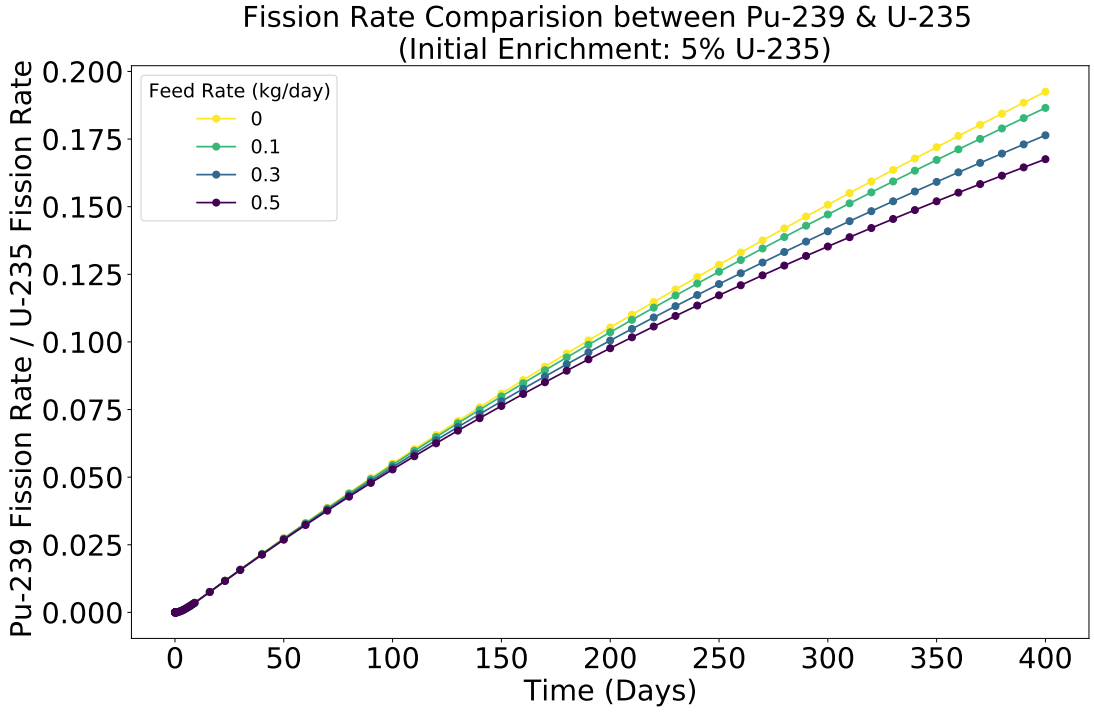

(b) Initial Fuel Salt Enrichment of 5% U-235

Figure 5.2: The fission rate ratio between Pu-239 and U-235 for varying feed rates of uranium.

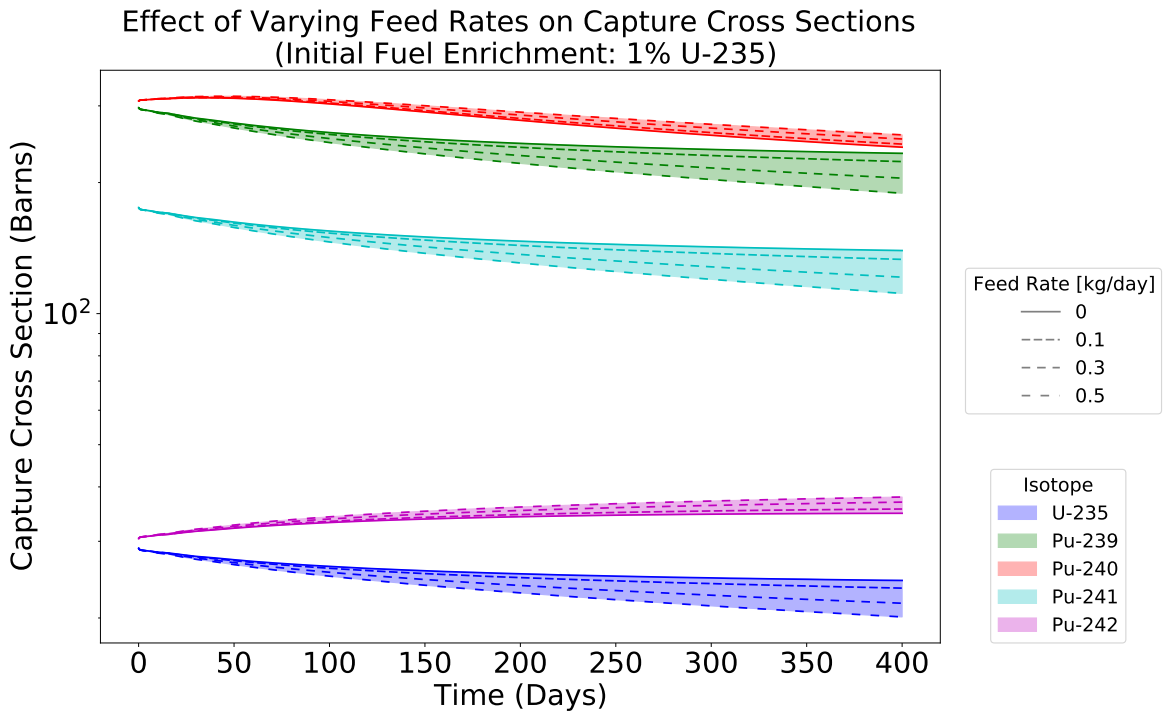

(a) Initial Fuel Salt Enrichment of 1% U-235

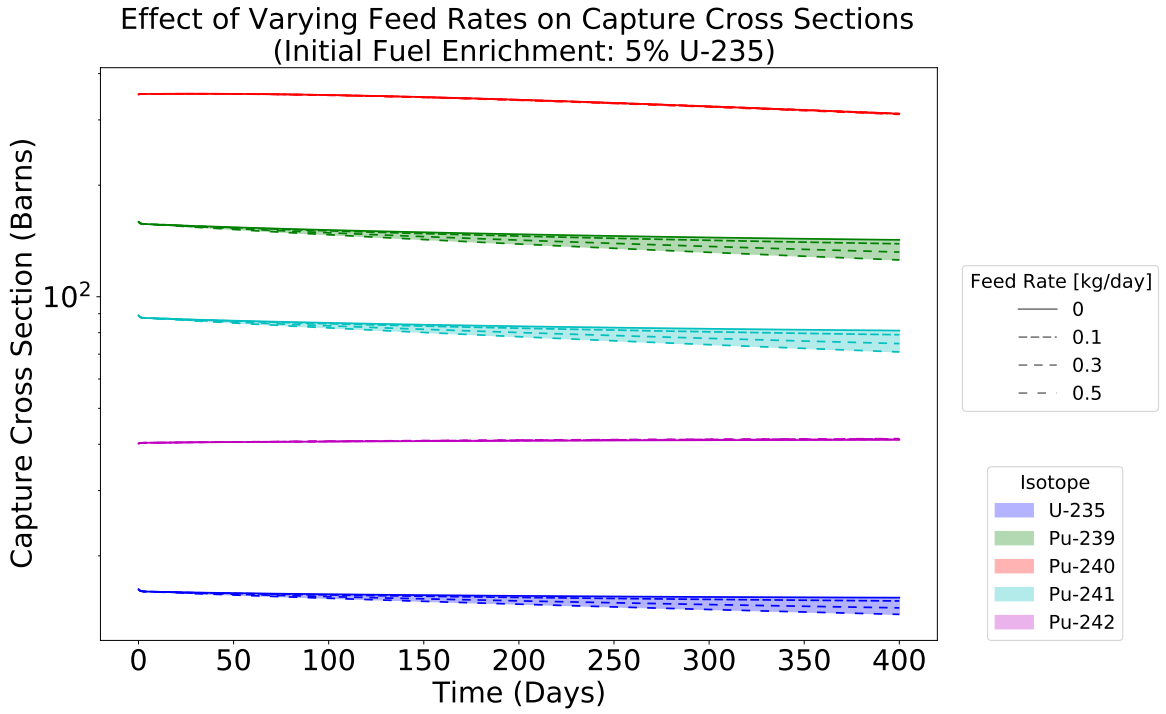

(b) Initial Fuel Salt Enrichment of 5% U-235

Figure 5.3: The capture cross-sections for select isotopes for varying feed rates of uranium.

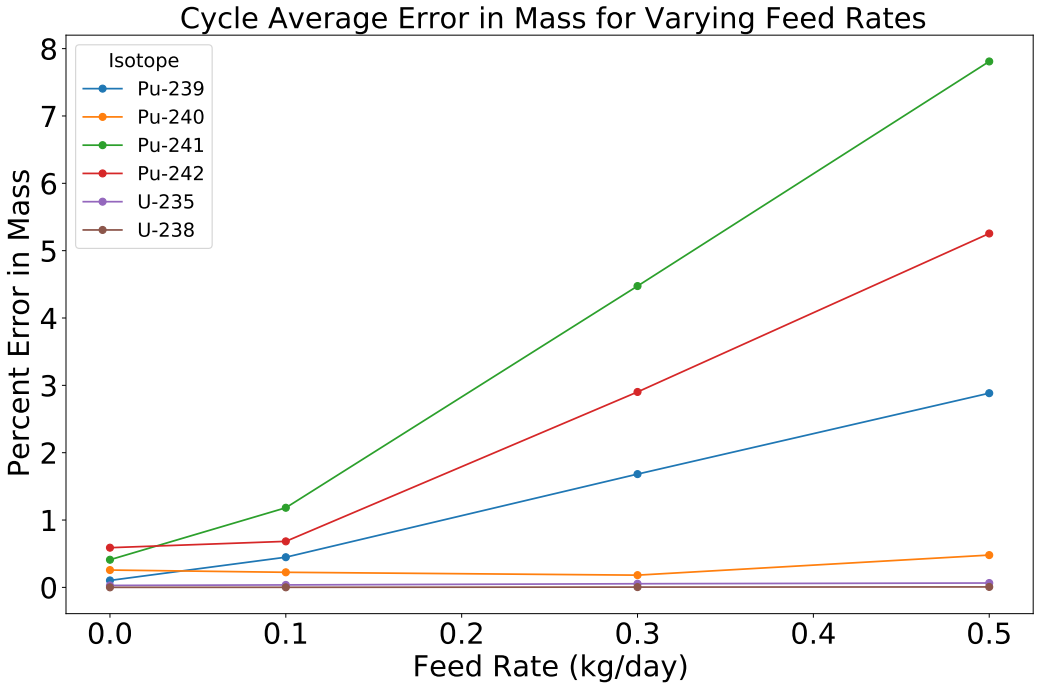

Figure 5.4: Cycle average error in mass between ORIGEN and TRITON solutions for varying feed rates. The ORIGEN library was generated with no uranium feed and an initial fuel enrichment of 3% U-235.

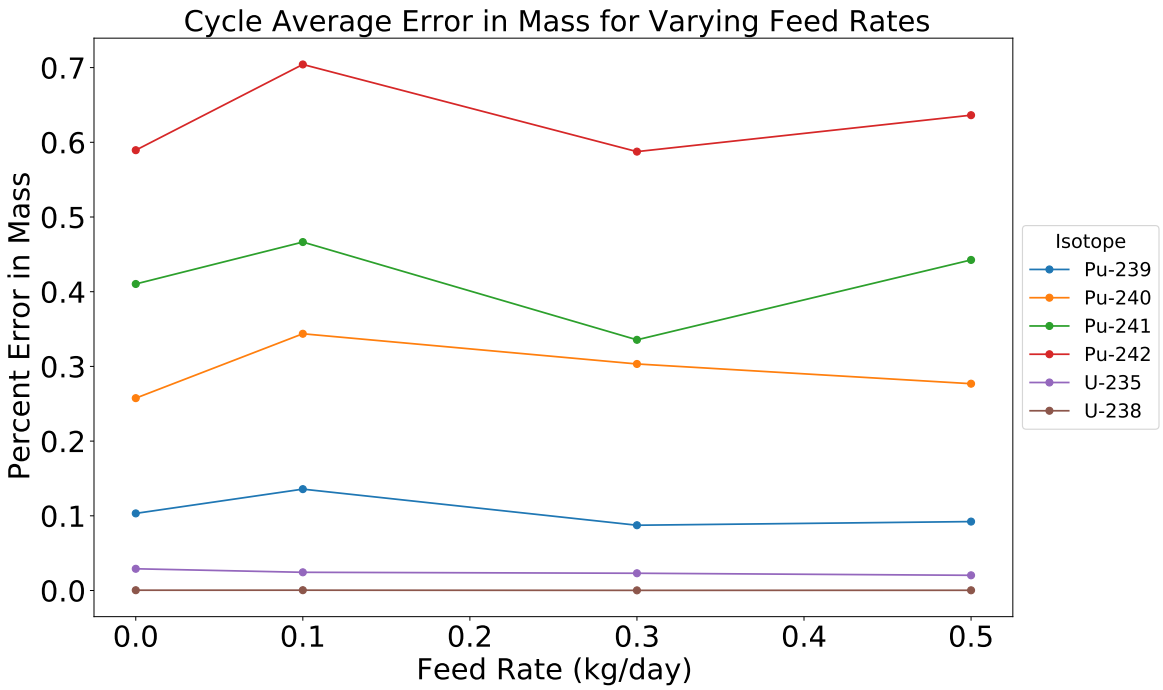

Figure 5.5: Cycle average error in mass between ORIGEN and TRITON solutions for varying feed rates.

5.4.2 Initial Fuel Enrichment and Feed Rate Interpolation

Figure 5.6 shows the interpolation error from interpolation over both initial enrichment and feed rate. Four libraries were used for interpolation at enrichments of 0.2 and 0.4 (w.t. % U-235), and at feed rates of 0 and 0.5 (kg/day). The error for the plutonium isotopes is significantly higher than when only feed rate was interpolated. The highest error is again seen for the higher plutonium isotopes.

Figure 5.7 shows the interpolation error from interpolating over initial enrichment for varying uranium feed rates. In this case eight libraries were used with enrichments of 0.2 and 0.4 (w.t. % U-235), and at feed rates of 0, 0.1, 0.3 and 0.5 (kg/day). The errors in this case are extremely close to the previous case. This suggests that the driving cause of error in interpolation is from the interpolation over the initial fuel enrichment and not the feed

rate. Additionally, it shows that there is no benefit from generating libraries at 0.1 and 0.3 (kg/day) if initial fuel enrichment is to be interpolated over.

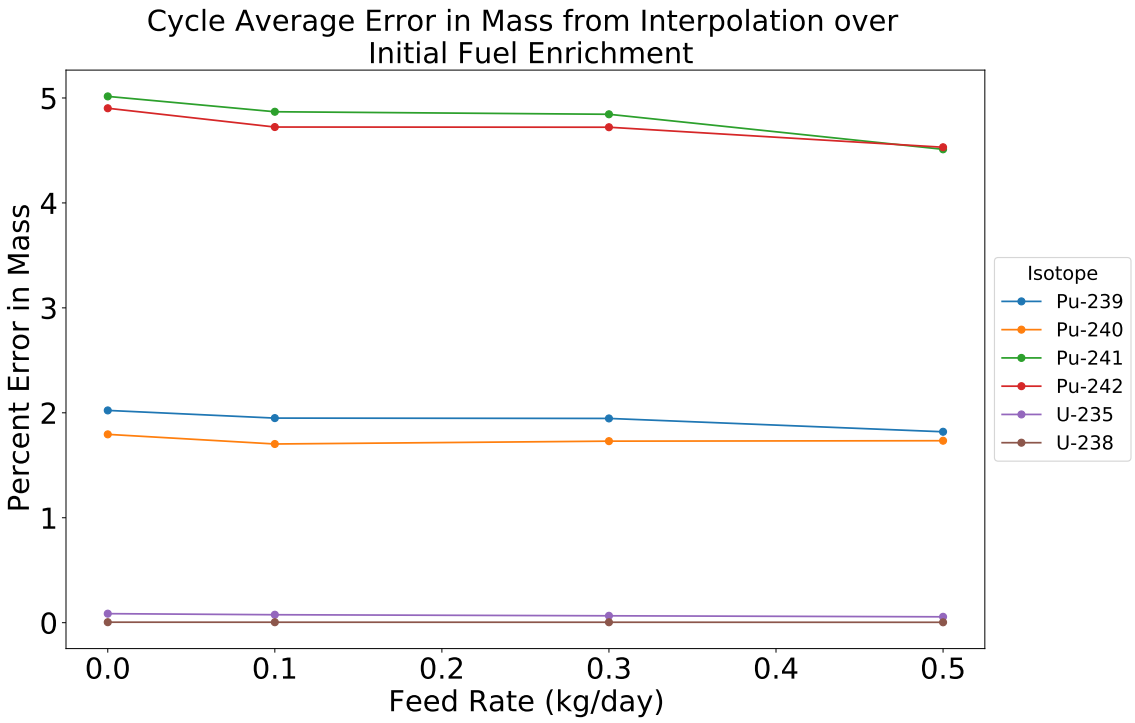

Figure 5.6: Cycle average error in mass from interpolation over initial enrichment and feed rate at varying uranium feed rates. The initial enrichment of all cases is 3% U-235 and is interpolated from libraries of 2% and 4% U-235. The feed rates at 0.1 and 0.3 (kg/day) are interpolated from libraries at 0 and 0.5 (kg/day).

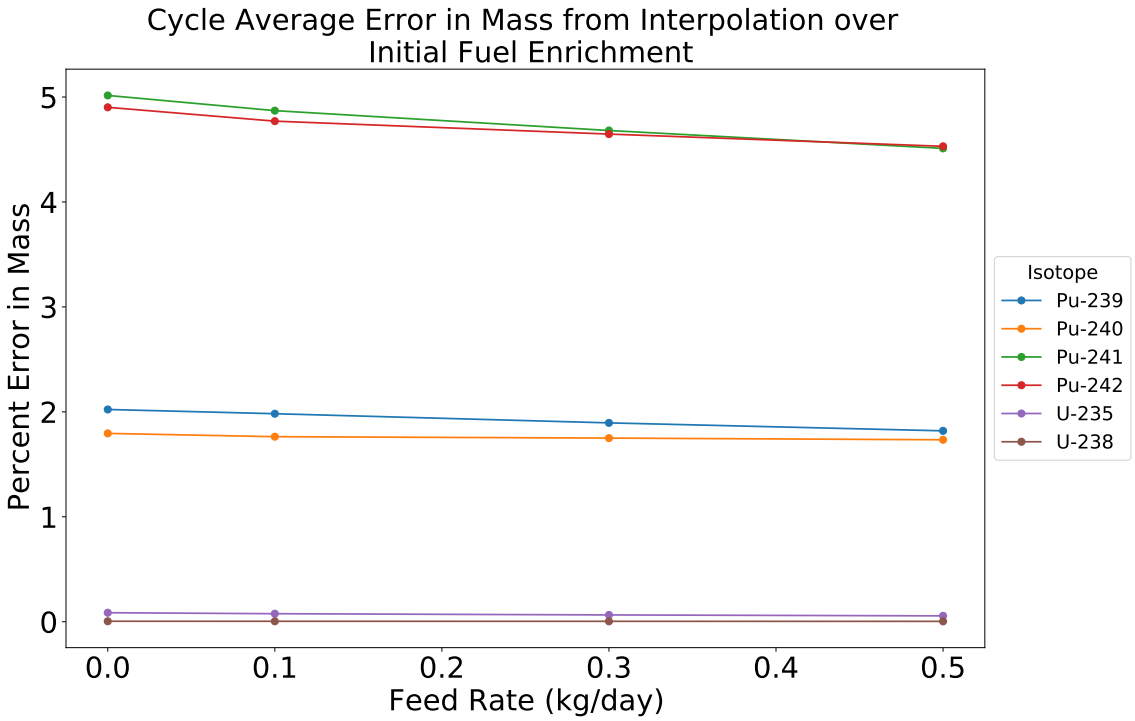

Figure 5.7: Cycle average error in mass from interpolation over initial enrichment for varying uranium feed rates. The initial enrichment of all cases is 3% U-235 and is interpolated from libraries of 2% and 4% U-235.

Chapter 6

Summary and Conclusions

6.1 Summary

This thesis detailed methodology for creating ORIGEN reactor libraries for liquid-fueled molten salt reactors. In the first part of the work a methodology for generating and spacing libraries for static MSRs was detailed. This methodology was based on analyzing the reaction coefficients of the transition matrices of libraries. The absolute difference in transition matrix values were minimized to create multiple spacing configurations. A test case was shown using libraries for a single-fluid thermal fluoride salt reactor. Additionally, a robust code framework was developed to generate and space these libraries for different reactor designs than the ones analyzed.

In the second part of the work fission product processing was incorporated into the reactor libraries. Two types of fission product processing were added: gas sparging which removed gaseous and non-dissolved metal fission products, and salt processing which removed Lanthanides and other soluble fission products. The effect of the fission product processing on the reactor system was extensively studied. It was then shown that the removal of fission products from a single system could be captured using interpolation over effective one-group removal cross-sections. Finally, it was shown the removal of fission products from both systems could be captured using a similar interpolation scheme.

The final part of the work incorporated online refueling into the reactor libraries. The effect of varying initial fuel enrichment of the system and refueling feed rate were studied.

It was then determined that refueling could be captured in the libraries and be interpolated over.

6.2 Conclusions

The use of ORIGEN reactor libraries to simulate liquid-fueled molten salt reactors appears promising. If created in a rigorous manner the libraries can quickly simulate a variety of designs including those with material feed and removal. To expand upon this work additional reactor designs should be tested with the presented generation and spacing methodology. Additionally, fission product processing and online refueling should be combined together and included in the spacing methodology. Finally, validation data for the isotopics of a variety of MSR designs would be immensely useful.

Bibliography

[1] Ashraf, O., Rykhlevskii, A., Tikhomirov, G. V., and Huff, K. D. (2020). Whole core analysis of the single-fluid double-zone thorium molten salt reactor (SD-TMSR). *Annals of Nuclear Energy*, 137:107115. 34

[2] Bettis, E. S., Schroeder, R. W., Cristy, G. A., Savage, H. W., Affel, R. G., and Hemphill, L. F. (1957). The Aircraft Reactor Experiment—Design and Construction. *Nuclear Science and Engineering*, 2(6):804–825. 5

[3] Boyd, S. and Taylor, C. (2017). *Chemical fundamentals and applications of molten salts*. Elsevier Ltd. 7

[4] C. E. Till (1979). Denatured Fuel Cycles. In *International Conference on Nuclear Cross Section for Technology*. 9

[5] Finne, J., Picard, G., Sanchez, S., Walle, E., Conocar, O., Lacquement, J., Boursier, J. M., and Noel, D. (2005). Molten salt/liquid metal extraction: Electrochemical determination of activity coefficients in liquid metals. *Journal of Nuclear Materials*, 344(1-3):165–168. 13

[6] Haubenreich, P. N. and Engel, J. R. (1969). Experience with the Molten-Salt Reactor Experiment. *Nuclear Applications and Technology*. 17

[7] Hellesen, S. G. and Carl (2017). *Nonproliferation and safeguards aspects of the MSR Fuel Cycle*. Elsevier Ltd. 9

[8] Holcomb, D. E., Flanagan, G. F., Patton, B. W., Gehin, J. C., Howard, R. L., and Harrison, T. J. (2011). Fast Spectrum Molten Salt Reactor Options. Technical Report July, Oak Ridge National Laboratory. 10

[9] International Atomic Energy Agency (1970). Neutron Fluence Measurements. Technical report, International Atomic Energy Agency. 5

[10] International Atomic Energy Agency (2005). Thorium fuel cycle—Potential benefits and challenges. Technical Report May, International Atomic Energy Agency. 8

[11] International Atomic Energy Agency (2020). Advanced Reactors Information System (ARIS). https://aris.iaea.org/. viii, 5

[12] Leal, L. C., Hermann, O. W., Bowman, S. M., and Parks, C. V. (1999). Automatic rapid process for the generation of problem-dependent sas2h/origen-s cross-section libraries. *Nuclear Technology*, 127(1):1–23. 16

[13] LeBlanc, D. (2010). Molten salt reactors: A new beginning for an old idea. *Nuclear Engineering and Design*, 240(6):1644–1656. 8

[14] Lizin, A., Tomilin, S., Ponomarev, L. I., Fedorov, Y. S., and Hirose, Y. (2017). *Fast-spectrum, liquid-fueled reactors*. Elsevier Ltd. viii, 11

[15] Merzlyakov, A., Afonichkin, V., Shishkin, V., Sannikov, I., Uglov, V., Ignatiev, V., Bovet, A., Kormilitsyn, M., Toropov, A., Subbotin, V., Gnidoi, I., Khokhlov, V., Lizin, A., Surenkov, A., Zagnitko, A., Feynberg, O., and Osipenko, A. (2013). Molten salt actinide recycler and transforming system without and with Th–U support: Fuel cycle flexibility and key material properties. *Annals of Nuclear Energy*, 64:408–420. 8

[16] Moser, D., Wheeler, A., and Chvála, O. (2017). Lattice optimization for graphite moderated molten salt reactors using low-enriched uranium fuel. *Annals of Nuclear Energy*, 110:1–10. 18, 19

[17] Rearden, B. T. and M. A. Jessee, E. (2018). SCALE Code System, ORNL/TM-2005/39, Version 6.2.3. Technical report, Oak Ridge National Laboratory, Oak Ridge, Tennessee. Available from Radiation Safety Information Computational Center as CCC-834. 15, 21

[18] Robertson, R. C. (1965). MSRE Design and operations report : Part I - Description of reactor design. Technical report, Oak Ridge National Laboratory. 8

[19] Saltarella, P., Ott, L., and Yonder, G. (2004). Physical properties and correlations for the molten salt FLIBE and their implementation in the RELAP5/ATHENA thermal-hydraulics code. Technical report, Oak Ridge National Laboratory Nuclear Science and Technology Division. 6

[20] Scarlat, R. and Andreades, C. (2017). *Solid fuel, salt-cooled reactors*. Elsevier Ltd. 3

[21] Scott, C. D. and Carter, W. L. (1966). Preliminary Design Study of a Continuous Fluorination-Vacuum Distillation System for Regenerating Fuel and Fertile Streams in a Molten Salt Breeder Reactor. Technical report, Oak Ridge National Laboratory. 14

[22] Sly, N. C., Skutnik, S. E., and Wieselquist, W. A. (2015). Portable reactor data library interpolation via self-describing origen libraries. *Transactions of the American Nuclear Society*, 113(1):368–371. 16

[23] Transatomic Power Corporation (2016). Technical White Paper v 2.1. Technical report, Transatomic Power Corporation. 5

[24] Uhlíř, J. (2017). *Chemical processing of liquid fuel*. Elsevier Ltd. 11

[25] Williams, D. F. and Britt, P. F. (2017). Technology and Applied R&D Needs for Molten Salt Chemistry:Innovative Approaches to Accelerate Molten Salt Reactor Development and Deployment. Technical report, US Department of Energy, Office of Nuclear Energy. 6

[26] Williams, D. F., Toth, L. M., and Clarno, K. T. (2006). Assessment of Candidate Molten Salt Coolants for the Advanced High-Temperature Reactor (AHTR). Technical Report March, Oak Ridge National Laboratory, Nuclear Science and Technology Division. 7

[27] Worrall, L. G., Worrall, A., Flanagan, G. F., Croft, S., Krichinsky, A. M., Pickett, C. A., McElroy Jr, R. D., Cleveland, S. L., Kovacic, D. N., Whitaker, J. M., and White-Horton, J. L. (2016). Safeguards considerations for thorium fuel cycles. *Nuclear Technology*, 194(2):281–293. 9

[28] Yoshioka, R. and Kinoshita, M. (2017). *Liquid fuel, thermal neutron spectrum reactors*. Elsevier Ltd. 6

Appendices

A Project Code

The code for this project is available on GitHub (https://github.com/keanderson35/MSR-ORIGEN-Libraries). All code for the project is written in Python 3.7. This appendix is divided into three sections: Semi-Generic-MSR, SCALE Tools, and Analysis. The Semi-Generic-MSR section describes the code that is used to create TRITON inputs that generate the ORIGEN reactor libraries. The SCALE Tools section describes code used to both run SCALE and analyze its output from Python. Finally, the Analysis section describes the code used to analyze the ORIGEN reactor libraries. More detailed documentation of the functions and classes listed can be found within the code itself. Additionally, code that is not described here but is within the GitHub repository include: the code used generate all inputs, plotting scripts, and the code used to generate final results.

A.1 Semi-Generic-MSR

The Semi-Generic-MSR package includes classes to generate TRITON input scripts for hexagonal pitched, square pitched, and homogeneous reactors. Model parameters are passed through dictionaries during the creation of a class object. Parameter dictionaries that include info for geometry, materials, depletion, TRITON controls, and file controls must be passed to the object. Optional parameters can also be passed to the object for creating material timetables (fission product processing / online refueling), material hold tanks (required for removal of fission products), and shell commands (for coping TRITON files from SCALE's temporary working directory).

Include in the package is a variety of material definitions that can be imported including FLiBe, graphite, air, steel, lead, and argon. The material definitions are all constant expect for FLiBe which requires an input for U-235 enrichment. More detail about the materials (temperatures, densities, etc.) can be found within the code.

The following example shows the creation of a single TRITON run for a single channel model with fission product removal. The class and material definition code are shown as "imports" due to their length. The actual code for them can be found in the code repository.

```
# ------------------------ Begin Example Input ------------------------

from Semi_Generic_MSR.Input_Generation.HexagonalMSR import \
    SingleChannelHexagonalMSR
from Semi_Generic_MSR.Input_Generation.Materials import \
    graphite, flibe_salt, argon

triton_params = {
        'run_name': 'MSR - Material Addition & Removal',
        'cross_section_library': 'scale.rev05.xn252v7.1',
        'run_parameters': None
}

geometry_params = {
        'reactor_geometry': 'single_channel',
        'channel_radius': 2.7282,
        'channel_pitch': 7.5,
        'mesh_points': 30
}

material_params = {
        'salt_material': flibe_salt(0.05),
        'reflector_material': graphite,
        'material_depletion': [1]
}

depletion_params = {
        'power': [20],
        'depletion_length': [3000],
        'depletion_steps': [100]
```

```
}

tank_params = {
        'material_numbers': [3],
        'materials': [argon],
        'depletion': [3]
    }

file_params = {
        'file_base_name': "MSR-MAR-A-Example"
        'save_folder': "C:/"
}

he_bubbling_isotopes = "H He N O Ar Kr Nb Mo Tc Ru Rh Pd Ag" \
                       "Sb Te Xe Lu Hf Ta W Re Ir Au"

removal_rate = 3.333E-01
removal_constant_list = [removal_rate] * 23

flow_1 = {
        'from_material': 1,
        'to_material': 3,
        'flow_type': 'continuous',
        'flow_units': 'pers',
        'nuclide_list': he_bubbling_isotopes,
        'removal_constant_list': removal_constant_list,
        'time_list': [0.0],
        'factor_list': [1.0]
}
```

```
timetable_params = [flow_1]

MSR_MAR_A = SingleChannelHexagonalMSR(file_params, geometry_params, \
    material_params, depletion_params, triton_params, timetable_params, \
    tank_params)

MSR_MAR_A.write_triton_input()
MSR_MAR_A.write_pbs_script()
MSR_MAR_A.generate_files()

# ------------------------ End Example Input ------------------------
```

A.2 SCALE Tools

The SCALE Tools code includes a variety of functions and classes to make running and analyzing SCALE output easier. A brief description of these functions and classes is included below. The SCALE Tools directory is composed of five different sub-directories: Derived, f71, OBIWAN, ORIGEN, and TRITON. The latter four directories included code for running and analyzing SCALE program named as such. The derived directory includes code that utilizes multiple SCALE programs to calculate values available from a single program (such as reaction rates).

Functions

calculate_reaction_rate: This function calculates the reaction rate from a f71 material file and f33 library file.

read_f71_file: This function reads a f71 file by running the SCALE module 'f71tocsv'.

interpolate_reactor_libraries: This function interpolates two reactor libraries using OBIWAN.

read_obiwan_cross_sections: This function reads 1-group cross sections from an ORIGEN f33 file.

read_f33_loss_cross_sections: This function reads loss cross-sections from a f33 file.

read_f33_capture_cross_sections: This function reads capture cross-sections from a f33 file.

calculate_effective_one_group_cross_section: This function calculates an effective one-group cross-section for an isotope from a f33 and f71 files.

calculate_element_one_group_cross_section: This function calculates an effective one-group cross-section for an element from a f33 and f71 files.

tag_data_library: This function tags a TRITON generated library for interpolation.

run_origen_point_depletion: This function runs an ORIGEN point depletion case using a given f33 library. A material definition, times-steps, and power profile are required.

Classes

ORIGENOutputReader: This class reads output from an ORIGEN calculation. Available output includes calculation time-steps, reactor power, total reactor flux, k-inf, and a dataframe of isotope masses.

TRITONOutputReader: This class reads output from a TRITON calculation. Available output includes calculation time-steps, reactor power, total reactor flux, flux spectrum, k-inf, transport-k, and a dataframe of isotope masses.

A.3 Analysis

The Analysis code includes a variety of functions and classes for analyzing and spacing ORIGEN reactor libraries. A brief description of these functions and classes is included below. The Analysis code is broken in to three directories: Transition Matrix Analysis,

Multi-Library Analysis, and Library Spacing. The Transition Matrix Analysis directory includes code to read in and analysis the transition matrices generated from TRITON. The Multi-Library Analysis directory includes code to easily analyze multiple reactor libraries at once. Finally, the Library Spacing directory include code to space the reactor libraries.

Functions

generate_coefft_table: This function generates a transition coefficient table from an f33 file using OBIWAN.

import_transition_matrix: This function imports a transition coefficient table into a pandas dataframe.

filter_transition_matrix: This function filters a transition coefficient dataframe to only relevant reaction pathways.

load_transition_matrices: This function searches for a filtered version of the transition matrix to load into a dataframe. If one cannot be found import and filter functions are run and the dataframe is saved into a pickle file. for easier

transition_matrix_average_relative_change: This function calculates the relative change between two transition matrices.

transition_matrix_absolute_difference: This function calculates the absolute difference between two transition matrices

interpolate_transition_matrix: This function interpolated filtered transition matrices.

tm_compare_interpolation: This function compares an interpolated transition matrix and a generated transition matrix.

Classes

MultiLibraryParser: This class allows multiple reactor libraries to be analyzed together. Methods in the class allow for: tagging multiple libraries at once, interpolating libraries, running ORIGEN calculations, calculating both time-dependent and time-averaged isotopes differences across libraries, calculating cross-sections across libraries, calculating fission rates ratios across libraries, and calculating flux and transport-k across libraries.

LibrarySpacer: This class includes the methods for calculating the spacing of reactor libraries. Two lower-level methods allow the difference in transition matrix values and the error in mass from interpolation to be calculated for a given parameter combination. Two higher-level methods can calculate the ideal parameter spacing given a parameter name and the number of parameter spacings to keep. Additionally, a method for generating the violin plots shown in Chapter 3 are included in the class.

Vita

Kyle Anderson was born in Texas to Mark and Kathryn Anderson. His only sibling is his older sister, Courtny. Kyle attended Olathe Northwest High School in Kansas, graduating in 2014. He attended the University of Wisconsin-Madison, graduating in May of 2018 with a B.S. in Nuclear Engineering and certificate in Mathematics. In the fall of 2018, he began working on a master's degree at the University of Tennessee in the Nuclear Engineering Department under his advisor Dr. Steven Skutnik. He graduates with a M.S. in Nuclear Engineering and a Nuclear Security Science and Analysis Graduate Certificate in the summer of 2020.